6. THE OBLIQUE SEISMIC EXPERIMENT ON DEEP SEA DRILLING PROJECT LEG 52

R.A. Stephen,[1] K.E. Louden, and D.H. Matthews, Department of Geodesy and Geophysics, University of Cambridge, Cambridge, England

SUMMARY

The first successful Oblique Seismic Experiment (OSE) in oceanic crust was carried out in Hole 417D. The OSE had been proposed to supplement the IPOD crustal borehole as a means of investigating seismic Layer 2. Specific objectives were to determine the lateral extent of the structures intersected by the borehole, to analyze the role of large cracks in the velocity structure, to look for anisotropy which may be caused by cracks with a preferred orientation, and to measure attenuation.

The best velocity model for the crust at Site 417, based on travel time and amplitude studies of the seismograms, consists of a constant velocity gradient throughout Layer 2 of 1.2 s^{-1} and 0.8 s^{-1} for P and S waves, respectively. Layer 2 is 1.3 km thick. The velocities at the bottom of Layer 2 correspond to those for uncracked basalt.

Anisotropy in either Layers 2 or 3 is not required by the data. Since the large fissures observed in the FAMOUS area should produce noticeable anisotropy, it appears that large fissures are not present in the studied crust (110 m.y.). The results agree with the theory that large fissures close with age and cracks close with depth. The experiment should be run again in younger crust for comparison with these results.

INTRODUCTION

Objectives

As conventional refraction and reflection experiments are designed to look at refracted and reflected rays, so the Oblique Seismic Experiment (OSE) is designed to look at "oblique" rays, that is, direct rays which impinge on the receiver at angles of incidence from 0° to almost 90°. In this study, this means receiving shots in a borehole which have been generated at the surface at small to large ranges (Figure 1).

The OSE was proposed to supplement the IPOD crustal borehole as a means of investigating oceanic Layer 2. The experiment has the following four objectives:

1) Determine the lateral extent of the structure intersected by the borehole.

2) Analyze the role of fissures and large cracks in the velocity structure of oceanic crust.

3) Look for anisotropy which may be caused by cracks with a preferred orientation.

4) Measure attenuation in oceanic crust.

[1]Present address: Woods Hole Oceanographic Institution, Woods Hole, Mass.

Structure of Layer 2

The range of refraction velocities for Layer 2 is substantially greater than the range for Layer 3 or the mantle. An average Layer 2 velocity was given by Raitt (1963) as 5.07 ±0.63 km/s, as opposed to a Layer 3 velocity of 6.69 ±0.26 km/s and a mantle velocity of 8.13 ±0.24 km/s. The larger deviation of Layer 2 velocities may be a result of the short range over which refractions from Layer 2 appear as a first arrival. However, Houtz and Ewing (1976) split Layer 2 into three layers and divided observations into three geographical regions (Reykjanes Ridge, Atlantic Ocean, and Pacific Ocean). The standard deviations for the top two layers, 2A and 2B, (±0.4 km/s) are still much larger than for Layers 2C and 3 (±0.2 km/s). Since the observational problems for Layers 2A, 2B, and 2C are about the same, it appears that at least some of the deviation in Layers 2A and 2B velocities can be attributed to real lateral velocity changes.

Hyndman (1977), using data for DSDP Hole 332B, obtained a reasonable refraction velocity from the time-weighted average of basalt velocity from cores and an estimated sediment-rubble velocity. His model for upper Layer 2 consists of fractured basalt with intercalated sediment rubble. A measure of the extent of fracturing is calculated from the drilling rate. Since drilling rate changes

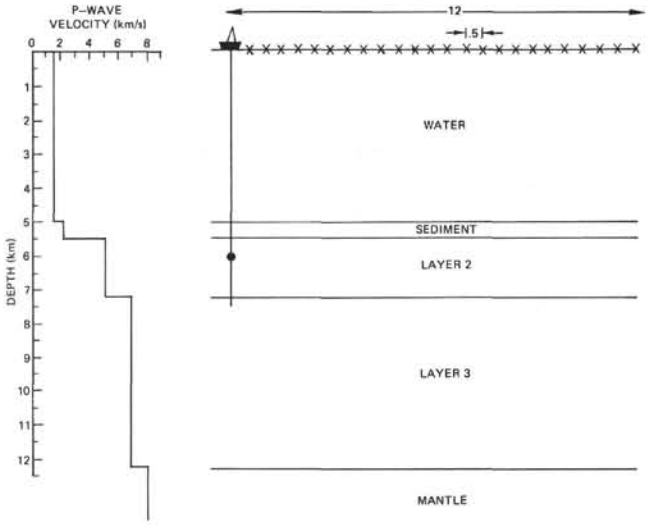

Figure 1. *Layout for the Oblique Seismic Experiment over average oceanic crust (Ludwig et al., 1970). The dot represents a receiver depth of 6 km and the crosses indicate the recommended shooting program for the OSE over oceanic crust.*

significantly between holes only a short distance apart, it would appear that significant changes in effective refraction velocity can occur over ranges on the order of 100 meters.

The velocity measured by conventional refraction experiments is an average over the range of arrivals, and the method requires ranges of 2 km or more to identify the refractor (Raitt, 1963; Houtz, 1976). Since the OSE can obtain velocities from direct wave arrivals and is able to look at lateral velocity changes in Layer 2 at distances less than 1.0 km from the hole, it can link the borehole structure observed by logging and core studies with the surface-to-surface refraction work which defines the basic structure of oceanic crust. No conventional refraction work was performed at Site 417; however, a comparison between the OSE results and the logging and core studies can be made (Salisbury et al., this volume, Part 2).

Significance of Cracks in Oceanic Crust

The nature of cracks in oceanic crust is important for two reasons. First, cracks provide channels for hydrothermal circulation. The depth and extent of this circulation has consequences in the study of oceanic heat flow (Hyndman et al., 1977). Also, an understanding of the formation of mineral concentrations by hydrothermal action would have economic consequences in deep-sea mining (Lister, 1974). The second reason for studying cracks is to see if they are directly responsible for any seismic discontinuities. This knowledge would lead to a better understanding of the process of sea-floor spreading and the formation of oceanic crust (Lort and Matthews, 1972).

Voids in the oceanic crust are envisaged on three scales: pores and microcracks (Brace et al., 1972), vugs (pores too large to be present in cores), and large fissures (Ballard et al., 1975). Ultrasonic measurements on hand samples in the laboratory should be able to predict the effect of microcracks on velocity *in situ*, and sonic logging in oceanic crustal boreholes should determine the effects of vugs on velocity. However, only detailed seismic experiments such as the OSE can determine the effect of large fissures. Salisbury et al. (this volume, Part 2) discuss the sizes and relative abundances of cracks from seismic measurements at Site 417.

Anisotropy

Oceanic crust is formed by a bilaterally symmetric process and any study of oceanic crustal structure should consider the possibility of azimuthal velocity anisotropy. That oceanic crust may be anisotropic is suggested by the presence of anisotropy in the oceanic upper mantle caused by preferred crystal orientation (Hess, 1964). The most likely source of Layer 2 anisotropy is preferred crack orientation (Ballard et al., 1975; Ballard and van Andel, 1977; Macdonald and Luyendyk, 1977; Luyendyk and Macdonald, 1977). Both mechanisms could be the result of the same stress field.

Detailed studies at the Mid-Atlantic Ridge (Macdonald and Luyendyk, 1977; Ballard and van Andel, 1977) show extremely well defined, preferred crack orientations. The standard deviation of crack orientation at one site in the inner floor studied by Macdonald and Luyendyk was only 6°. As the crust moves outward, it is uplifted in a series of normal faults to the rift mountains which again are remarkably well oriented.

Estimates of the effect of preferred crack orientation on velocity can be obtained from the theoretical work of Anderson et al. (1974). Their table 2 gives shear and compressional wave velocities normal and parallel to cracks of various densities and aspect ratio.

The FAMOUS area work shows many faults and fissures in the median valley (Ballard and van Andel, 1977). In the central volcanic province, 36 fissures and 14 faults were crossed during 3.8 km of traverses; in the marginal tectonic province, 71 fissures and 80 faults were crossed in 7.5 km of traverses; and in the west wall province, 18 faults were crossed in 1.9 km of traverses. In the west wall province, some faults and fissures may have been covered with sediment. Vertical movement at the walls seemed to occur at the fissures. One fissure crossed in the marginal tectonic province was 50 cm wide and at least 50 meters long, giving a minimum aspect ratio of 0.01.

Based on these observations, we can construct a sample model for the upper crust. Let us take one spheroidal fissure, 50 meters in length, with an aspect ratio of 0.01 in every 100-meter cube. The resultant porosity would be 1 per cent and the resultant velocity anisotropy (both P and S) should be greater than 0.2 km/s (cf. $\alpha = 0.05$, $\phi = 0.01$, $K_f = 20$ kbar in table 2 of Anderson et al., 1974).

The model may underestimate anisotropy because fractures associated with faults are not considered and the normal faulting in the mountain-building process may be expected to produce more oriented cracks. The estimate would be decreased if the fissures are filled with rubble or completely closed. The OSE should be able to detect this anisotropy if it is present.

Attenuation

Attenuation is the residual loss in amplitude with distance after consideration of divergence, and transmission and reflection losses at boundaries (White, 1965). It can be subdivided into intrinsic attenuation, which is a direct measure of the anelasticity of the rock, and residual attenuation, which is what is commonly measured and includes scattering effects caused by inhomogeneities (Hamilton, 1976). The causes of intrinsic attenuation are reviewed by Jackson and Anderson (1970) and Gordon and Nelson (1966). Residual attenuation is a worthwhile quantity in its own right in the interpretation of crustal structure using amplitude analysis (Kennett, 1975; Fowler, 1976b). It may also give a measure of inhomogeneity in the crust.

A measure of attenuation in marine basalts was reported by Neprochnov et al. (1967) and Neprochnov (1971), who gave attenuation coefficients from 0.02 to 0.05 db/mHz (Hamilton, 1976). The OSE is expected to supplement this measure of attenuation.

DATA ACQUISITION

Equipment

The borehole geophone used in the OSE is a modified Geo Space Wall-Lock seismometer (Geo Space Corp.,

1972). It has an electrically driven arm, which can be extended from the tool when it is in the open hole, to clamp the unit in place. A spring maintains pressure on the arm when the motor is switched off. This reduces the effect of pressure waves in the well (McDonnal et al., 1958; White, 1965; O'Brien and Lucas, 1971; Gal'perin, 1974) and isolates the tool from the ship's motion.

The Geo Space unit was purchased as a vertical component seismometer with a fixed-gain preamplifier which amplified the signals by 256 times (48 db). The OSE, however, requires a three-component system because the first P-wave arrival from large ranges has a horizontal motion. In addition, the background acoustic noise on *Glomar Challenger* is so high that the fixed-gain preamplifier is overloaded and testing is difficult. Consequently, we adapted the Geo Space seismometer to a three-component unit with variable gain preamplifiers (Stephen, 1977a). The gain could be changed at the surface to 0, 12, 24, 36, or 48 db. A seven-conductor logging cable transmitted the signals to the surface.

Shot ranges were computed from the direct water wave travel time to the *Glomar Challenger*. A hydrophone was suspended over the side to detect this arrival.

Operations

The Oblique Seismic Experiment was successfully completed in Hole 417D on 6 March 1977. The shooting was carried out by the *Virginia Key*, a research vessel from the Atlantic Oceanographic and Meteorological Laboratories of the NOAA (National Oceanic and Atmospheric Administration) in Miami.

The pattern shown in Figure 2 was fired with the geophone at 6060 meters BRF (below rig floor), and a single line from 12 km south-southwest of the *Glomar Challenger* to 12 km northeast was fired with the geophone at 5840 meters BRF. All charges were 20 pounds (~ 9 kg) of Tovex Extra. Fuses were cut to burn for 60 s, which gave a shot depth of approximately 46 meters. Shots were fired at 0.5-km intervals on the straight lines and at 2-km intervals on the arcs. The gain of the geophone preamplifier was constant at 48 db.

Data

An example of a raw record made during the shooting is shown in Figure 3. The signal-to-noise ratio of the records is generally good. The majority of the noise is caused by electrical switching on the ship and is the same on all three downhole channels (Figure 4). Since the P-wave is stronger on some channels than others, the signal-to-noise ratio can be improved by subtracting channels (Figures 4 and 5).

DATA ANALYSIS

Reduction

Corrections and Error Estimates

The greatest limitation in reducing explosive shot data is the flight-time correction:

$$\Delta t_f = \frac{1}{V_w}(V_c^2 + v_s^2)^{1/2} t_f$$

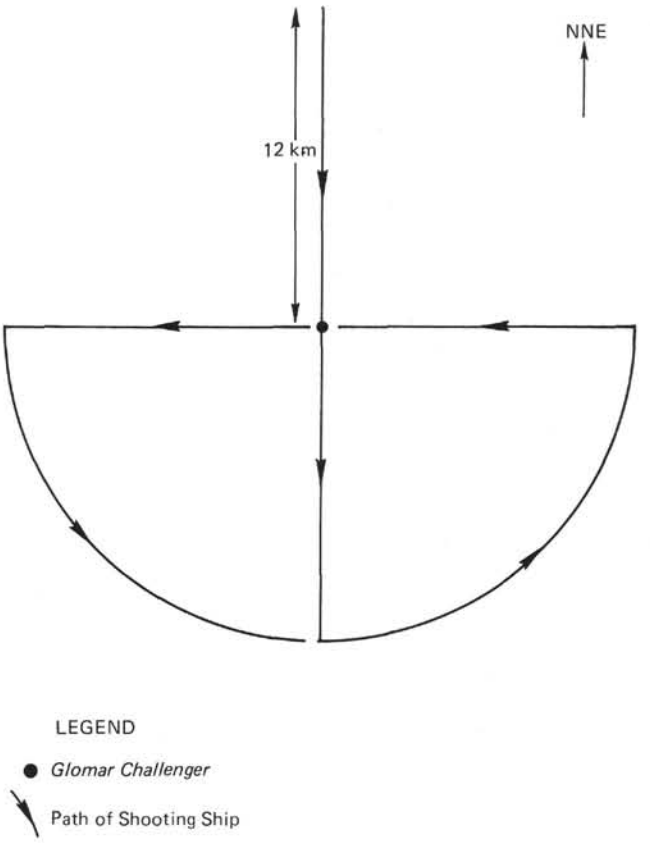

Figure 2. *Plan view of recommended shooting program. NNE is the direction parallel to the magnetic lineations at Site 417. Shots fired were at 0.5-km intervals on the straight lines and at 2.0-km intervals on the arcs. The straight line shots represent a minimum program to consider anisotropy and the arcs (ideally, a full circle) provide continuity.*

where V_w is the velocity of sound in water (= 1.540 ± 5 m/s), V_c is the sink rate of the charge (= 0.76 ± 0.15 m/s), V_s is the shooting ship's speed (= 2.60 ± 0.05 m/s), and t_f is the flight-time (= 60 ± 1 s). Typical corrections are 0.106 ± 0.005 s. Ship's speed was obtained from the time and range (uncorrected for flight time) between near and far shots on the same line. The *Virginia Key* slowed down for maneuvering around the *Glomar Challenger*, and flight-time corrections for the very near (< 0.75 km) shots are uncertain. The *Virginia Key*'s speed on the arcs was taken as the average speed of the two adjacent lines and is unreliable.

Ranges were picked from a plot of range versus the travel time from the shot to the hydrophone. This was computed by the ray-tracing technique for a model oceanic velocity gradient typical of the area and time of year (Maritime Information and Advisory Service, Godalming, U.K.). Radar ranges were logged during the experiment but were not as consistent as the ranges from travel time. Shot azimuths were monitored from the bridge during the experiment.

No correction was made for the drift of the *Glomar Challenger* relative to the beacon. Readings were taken

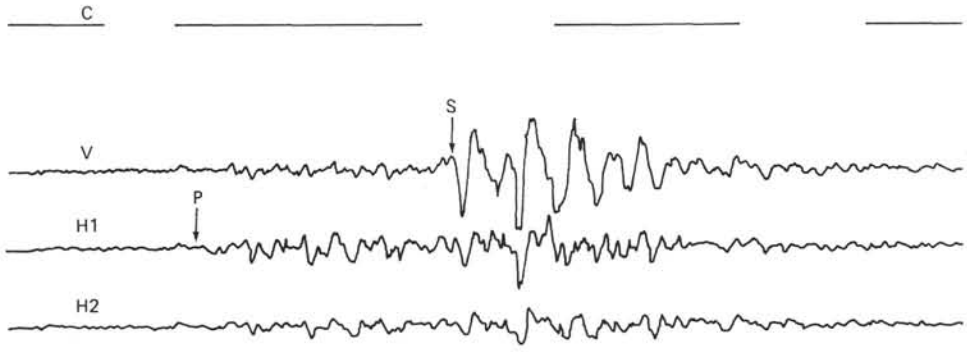

Figure 3. *Typical record for north-south line. Clock channel (C), vertical component signal (V), and the two horizontal component signals (H1 and H2) are shown as they were recorded onboard* Glomar Challenger. *The distance between right-hand ends of lines on the clock channel is 1 s. The strongest P-wave signal is arriving on the H1 component, which implies that the axis of this geophone is aligned approximately north-south. The angle of incidence of the arrivals is large, confirming that at long ranges the direct arrivals are traveling almost horizontally. This shot was fired at a range of 6.58 km on the north line with the geophone at 6060 meters below the rig floor.*

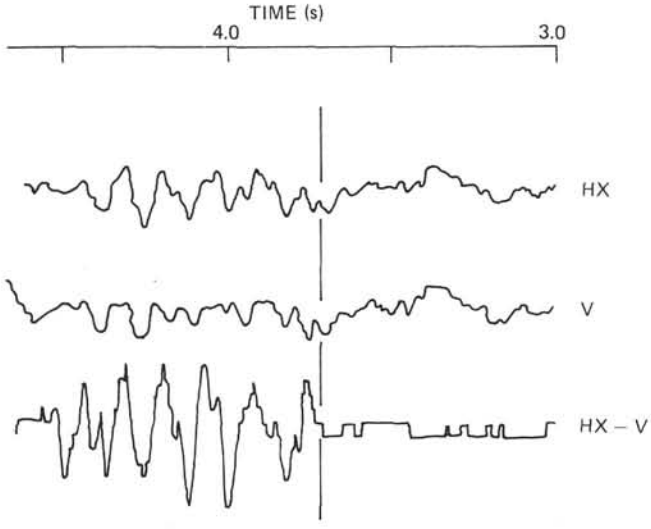

Figure 4. *Elimination of noise on downhole channels. Most of the noise on the geophone records is pick-up from motors on* Glomar Challenger *and is the same on all channels. In this case, HX has a stronger signal than V and the difference, HX-V, is almost pure signal. The steps to the right of the vertical time marker on the difference channel are the height of a single discrete amplitude step. The HX and V channels are shown at a different amplification than the HX-V channel.*

every 5 minutes, but did not change smoothly. There may have been a problem in the positioning computer.

Travel-time errors can be classified as relative errors, which are errors in times between shots, and absolute errors, which are errors in individual travel times. Examples of relative errors are timing and range errors (due to uncertainty in flight-time correction and charge sink rate) and errors in picking arrival times. Examples of absolute errors are phase shifts in the geophones and recording equipment and uncertainties in the following: (1) geophone and hydrophone depth, (2) offset of the hydrophone from the borehole, and (3) the velocity-depth profile of the ocean and sediments. Absolute travel times are not used in practice.

The tone break can be picked to 0.002 s, the geophone arrivals to 0.004 s, and the flight-time correction is good to within 0.012 s. If this is combined with an uncertainty in shot depth of 9.9 meters, the total estimated error for relative times is ± 0.025 s. Ranges are known to ± 24 meters. Errors associated with topography (Kennett and Orcutt, 1976) are considered in the data interpretation stage.

Record Sections

A complete set of record sections for the OSE is given in Appendix A. All the records, including the synthetic seismograms used for interpretation, have the same amplitude weighting. That is, up to 7 km, no weighting has been performed; over 7 km, the amplitudes have been multiplied by $(\text{range}/7.0)^{2.9}$. (This relationship was determined empirically to produce record sections of satisfactory appearance.) Direct comparison of amplitudes can be made between sections. Traces on the hydrophone records are normalized individually. (The maximum amplitudes of the traces are the same height.) No terrain corrections have been made on the sections.

The signal-to-noise ratio of the geophone records is generally good up to 10 km. At ranges greater than 10 km, the first arrival is sometimes obscured by noise.

The long-range P-wave arrivals are stronger on the horizontal components than on the vertical component, as would be expected for a compressional wave at large angles of incidence. In addition, the two horizontal components were almost aligned with the shooting pattern and the strongest P arrivals occur on horizontal X for the north and south lines and on horizontal Y for east and west lines. These components were used for the travel-time study.

The *Virginia Key* did not have operating/echo-sounding or seismic profiling gear, so bathymetry and basement topography underneath the lines were not obtained. In

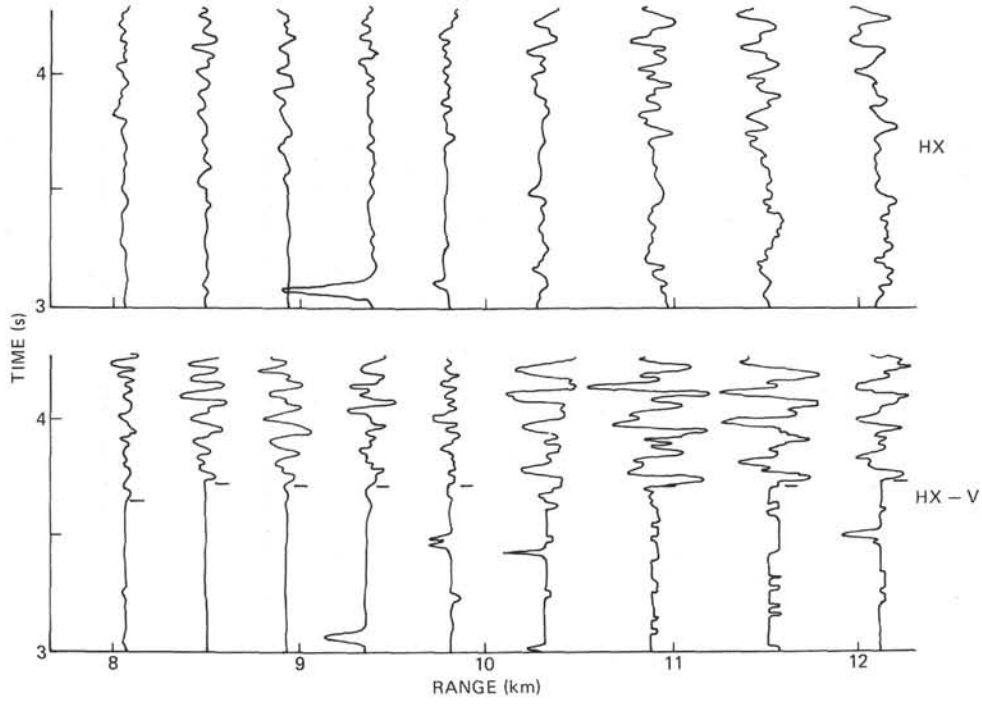

Figure 5. *Difference seismogram (HX-V) at long ranges compared to unmodified seismogram (HX) for the north line at the deep geophone position. It is generally easier to pick first P arrival times on the difference seismogram although amplitudes will be distorted. The HX section is weighted by (range/7.0)$^{2.9}$ but the amplitudes on the HX-V section bear no relation from trace to trace.*

addition, the hydrophone records from the *Glomar Challenger* are not suitable for determining basement arrivals. The hydrophone depth is about the same as the sediment thickness, and the sea surface reflection of the sea-bed arrival coincides with the first basement arrival. The interference makes picking accurate travel times impossible. Thus, basement topography was not determined during the experiment.

Seismic profiling had been performed in the area earlier by the *Glomar Challenger* and USNS *Lynch*. These lines were used for bathymetry and terrain corrections. Figure 6 shows their positions relative to the OSE lines. Figure 7 is an example of an actual profiling record.

Direct measurement of the sediment and Layer 2 velocities by laboratory studies of cores and sonic logging provides a basis for seismic modeling techniques. Table 1 outlines the significant depths in Hole 417D. Leg 51 drilled through 343 meters of sediment and 190 meters of basalt. Leg 52 extended the basement penetration to 366 meters. Cores were taken continuously for the bottom 150 meters of sediment and for all of the basalt. The sonic log was run from 148 to 447 meters sub-bottom.

Estimates of sediment velocity range from 1.57 km/s from the sonic log to 1.61 km/s from a study of reflected wave travel times. Core velocities between 200 and 280 meters sub-bottom are from 1.60 to 1.73 km/s (Site 417 Site Report, this volume). Because only 343 meters of sediment are present, the sediment velocity does not significantly affect relative travel times. A mean velocity of 1.60 km/s is considered representative. The strong mid-sediment reflection (Figure 7) is associated with a thin (16 m thick) clay layer at 156 meters sub-bottom (Site 417 Site Report, this volume) and log velocities at this point jump from 1.56 km/s to a maximum of 1.90 km/s. Twenty meters of high-velocity (1.67 km/s) chalk is present 10 meters above basement.

The mean laboratory velocity of basalt cores is 5.47 $\pm$ 0.02 km/s (a 23-m-thick massive basalt unit with a velocity of 5.75 km/s is present 70 m into the basement); the average density of the cores is 2.80 $\pm$ 0.05 g/cm^3; and the mean uncorrected sonic log velocity is 4.83 km/s (Salisbury et al., this volume, Part 2).

Data Interpretation — Travel Times

Initial Travel-Time Analysis

The first approach to the travel-time study was to model the times of the significant arrivals by trial and error. Only arrivals found to be consistent on all records were used. For direct and reflected arrivals, the travel-time curves were computed by ray-tracing through a model which included topography. The terrain corrections were only applied explicity to correct the critically refracted arrivals.

Figure 8 shows the travel-time curves superimposed on a sample record section. Although much of the information for constructing the curves came from difference seismograms (e.g., Figure 5) the best overall picture is obtained from an unmodified section.

The gradient was originally introduced at the top of Layer 2 in an attempt to explain the direct wave amplitude behavior. Synthetic seismogram analysis of the direct wave amplitudes failed to support it. The velocity for the bulk of

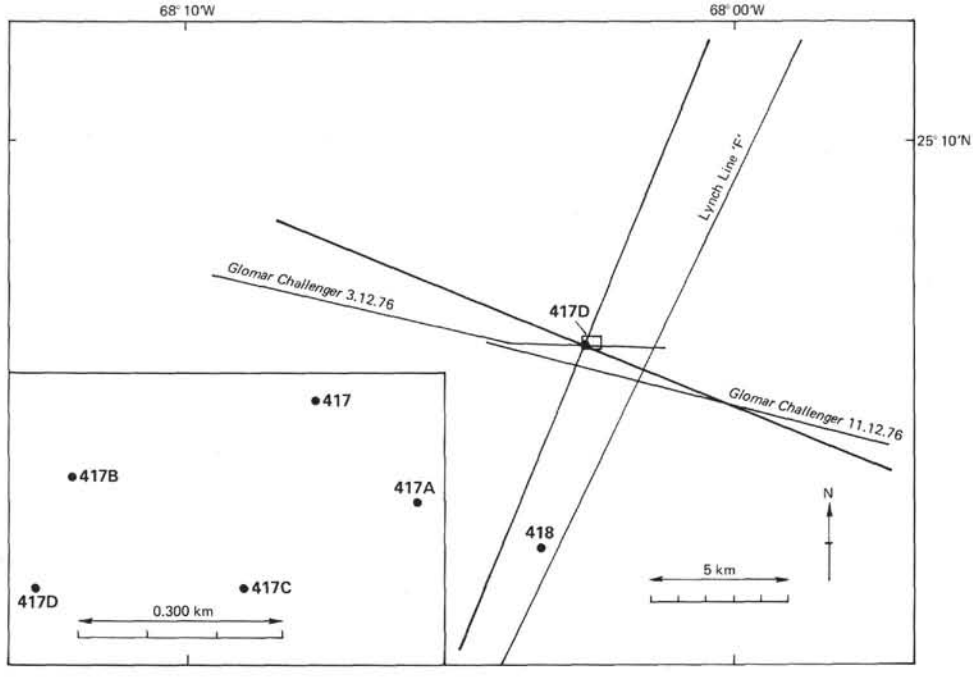

Figure 6. *Locations of the* Lynch *and* Glomar Challenger *profiles relative to the OSE lines. The inset shows the locations of the holes drilled at Site 417. Hole 417A reached basement at 5686 meters BRF compared to 5835 meters BRF for Hole 417D.*

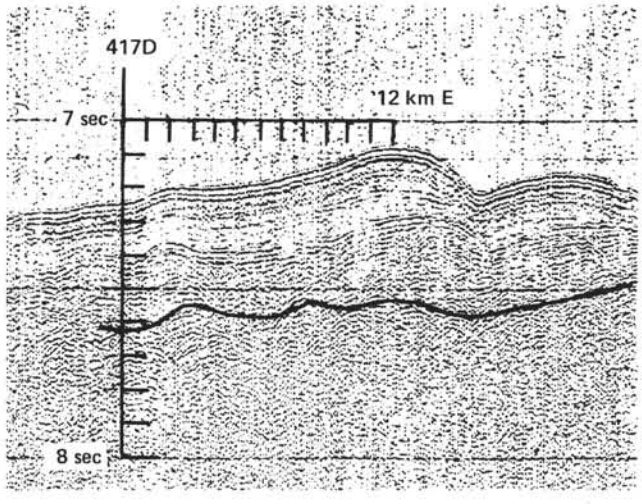

Figure 7. *Example of the* Glomar Challenger *profile used in the interpretation of the OSE data. The estimated location of the basement topography is shown by the thick black line. The strong mid-sediment reflector is evident about half-way between basement and the sea bed.*

Layer 2 of 5.25 km/s was chosen as the best general fit to the direct wave arrivals on all lines. (Time shifts due to small-scale topography were not considered.) The 6.8 km/s velocity, typical for Layer 3, was obtained from first arrivals between 5 and 9 km. Some arrivals in this region are either very weak or non-existent and their behavior changes significantly between lines. The 6.2 km/s layer above the 6.8 km/s layer is supported by relatively large first arrivals at large ranges (10 to 12 km). The velocity and depth were chosen by trial and error to produce the correct time difference between the 6.2 km/s refractor and the extrapolated 6.8 km/s refractor.

TABLE 1
Significant Depths in Hole 417D

	Depth From Rig Floor (m)	Depth From Mudline (m)	Depth Into Basement (m)
Sea level	10		
Mud line	5489		
Casing shoe	5515	26	
Sonic log-top	5637	148	
Basement	5832	343	
Geophone position 2	5840	351	8
Sonic log-bottom	5936	447	104
Leg 51 penetration	6022	533	190
Geophone position 1	6060	571	228
Depth to top of pipe	6092	603	260
Leg 52 penetration	6198	709	366

The S-wave velocities in Layer 2 were chosen to give the 3.75 km/s refraction the correct intercept. Depths for the S-wave case were taken from the P-wave model. In the OSE case, shear waves generally are displayed best on the vertical component seismograms (Appendix A).

Least-Squares Fit Analysis

To obtain more accurate velocities to look for azimuthal effects, linear regression by the least-squares method was performed on refracted P- and S-wave arrivals and on direct S-wave arrivals. The results of this study are summarized in Table 2. There is no significant evidence for azimuthally

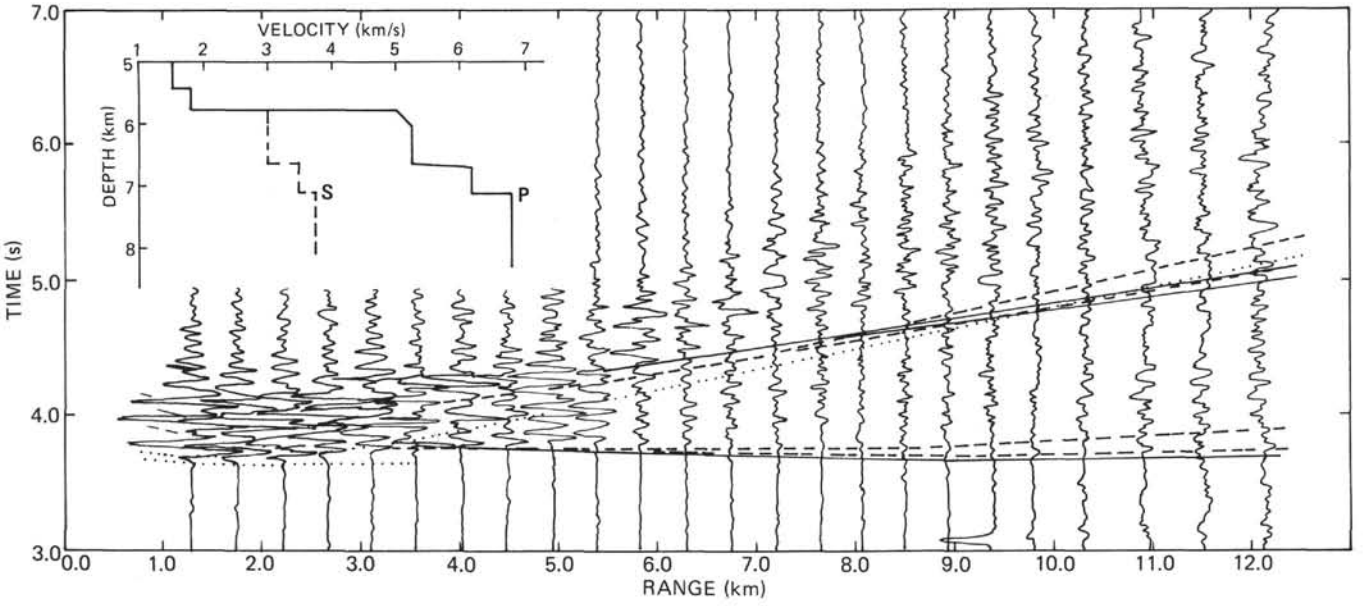

Figure 8. *Record section for the north line at the deep geophone position with the initial travel-time interpretation superimposed. Direct arrivals (....), reflections and refractions from the 6.2 km/s layer (---), and reflections and refractions from the 6.8 km/s layer (—) are shown for both P and S-waves. The direct P-wave arrival stops abruptly at 3.6 km because of the velocity gradient in the top of Layer 2. Travel times for arrivals between 7 and 12 km were picked from difference seismograms (e.g., Figure 5). The reflection curves from the 6.2 and 6.8 km/s layers were calculated using the ray tracing technique of Červený and Pšenčik and include terrain corrections. Bends in the refracted arrivals correspond to terrain corrections (Figure 7). The S-wave arrivals are clearer on the vertical component (Appendix A). In all of the figures, D is the depth of the geophone below the rig floor.*

in either P or S for Layer 3 or in S for Layer 2. The best estimate for Layer 3 compressional and shear velocities is highest in the north, lowest in the west, and about the same in the east and south. The changes in refracted velocity between the shallow and deep positions may be the result of constructive and destructive interference of first arrivals at the two depths.

The P and S refractions for Layer 3 give velocities which agree well with the initial model (6.7 and 3.71 km/s compared with 6.8 and 3.75 km/s). The direct S velocity is lower (2.60 km/s compared with 3.0 km/s), but this may be a consequence of an S-wave gradient in Layer 2.

Study of Direct Wave Arrivals and Small-Scale Topography

The short-range direct arrivals were used to determine the compressional wave velocity at the top of Layer 2. There are first arrivals only up to 5.0 km because Layer 2 is only 1.3 km thick. If the thickness of Layer 2 were 1.7 km (the mean thickness from Ludwig et al., 1970), the direct wave would be a first arrival to about 9.0 km (Stephen, 1977b).

Small-scale topography affects travel times considerably. Travel-time residuals between observed data and the data for a standard model with regional topography (Figure 7) are plotted in Figure 9. An upper Layer 2 velocity in this model of 4.8 km/s was selected because it gave the smallest time discrepancies between deep and shallow positions for the north and south lines. The upper Layer 2 velocity in the initial model is obviously too high.

The residuals can be attributed solely to the effect of small-scale basement topography. The east line shows the hill into which Hole 417A was drilled (Site 417 Report, this volume). An almost equally high hill appears to the west but it is less steep. In contrast, the north and south lines are flat, that is, the regional trend is valid. The south lines have significantly different residuals between 0.6 and 1.2 km. This may be because the two lines are about a kilometer apart. Some evidence for these small-scale features appears on the reflection profiles (Figure 7). Bumps in the mid-sediment reflector correspond roughly to the basement highs.

From the profiles and OSE data, it appears that Hole 417D was drilled in a trough between two steep hills having slopes of at least 10° and 26°, respectively. The topography is much less rugged parallel to the magnetic lineations than perpendicular to them, reminiscent of Mid-Atlantic Ridge topography (Ballard et al., 1975; Ballard and van Andel, 1977; Macdonald and Luyendyk, 1977). The hills are about 180 meters high.

There is no point in studying lateral velocity effects from direct arrivals unless the small-scale topography is known accurately from detailed profiling. Since sharp features on the sea bed are masked by diffractions (Laughton et al., 1960; Laughton, 1963; Spiess and Mudie, 1970), conven-

TABLE 2
Linear Regression Summary for the Six OSE Lines

Line (m)	Layer 3 P Velocity (refracted) (km/s)	Layer 3 S Velocity (refracted) (km/s)	Layer 2 S Velocity (direct) (km/s)
North -D = 6060	6.97 ±0.44 (6)	3.75 ±0.12 (11)	2.49 ±0.02 (5)
North -D = 5840	6.66 ±0.20 (7)	3.88 ±0.02 (6)	2.48 ±0.04 (6)
South -D = 6060	6.70 ±0.30 (11)	3.63 ±0.08 (8)	2.61 ±0.05 (4)
South -D = 5840	6.50 ±0.27 (7)	3.81 ±0.19 (5)	2.67 ±0.04 (3)
East -D = 6060	6.75 ±0.44 (8)	3.68 ±0.11 (6)	2.72 ±0.21 (4)
West -D = 6060	6.46 ±0.37 (8)	3.51 ±0.06 (7)	2.60 ±0.01 (4)
Means	6.67 ±0.34	3.71 ±0.10	2.60 ±0.06

Note: The number in brackets is the number of points used in the velocity determination.

tional reflection profiling may not be adequate in the deep ocean.

Data Interpretation — Amplitudes and Synthetic Seismograms

Introduction

Synthetic seismogram analysis of the data was conducted using the reflectivity method of Fuchs and Müller, (1971) modified for OSE geometry by Stephen (1977b). In this method, an appropriate source function must be assumed.

Comparison between the observed signals on the geophone channels at short ranges and the theoretical explosive source function (Fowler, 1976a) shows that the theoretical source is much shorter than the apparent direct arrival (Figure 10). Also, the first bubble pulse wavelet is greater than the initial wavelet. Both observations can be attributed to reverberations in the sediment. The time interval between the first two pulses is 0.19 s. An intra-sediment multiple would have this period if it occurred between horizons 0.15 km apart. Such a multiple could be generated between basement and the strong mid-sediment reflector on the reflection profiles (Figure 7). Unfortunately, attempts to model this effect failed because of numerical difficulties. The integrand in the integration evidently varies so quickly that numerical evaluation of the integral is impossible using reasonable increments (Stephen, 1977b).

It is unreasonable to expect that the extended waveform at short ranges could be caused by reflecting horizons below the receiver. To cause large reflections at short ranges, such horizons would necessarily be sharp and no evidence for sharp interfaces has previously been reported. Also, the nature of the waveform does not vary significantly at large ranges. Consequently, it is assumed that the waveform incident on the basement has the form of the short-range arrival (Figure 10).

Discussion

When compared with a typical line, e.g., Figure 11a, the synthetic seismogram based on the initial model in Figure 8 and shown in Figure 11b has a number of limitations, including the following:

1) The P-wave amplitudes in the critical region (4.5 to 5.5 km) are too weak (Region A in the figures).

2) The critically refracted P-wave arrival does not die away after 9.0 km (Region E).

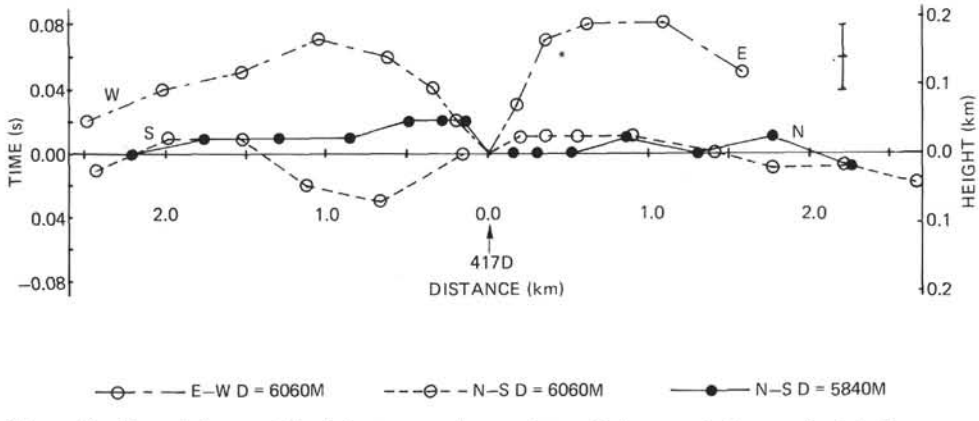

Figure 9. *Travel-time residuals between observed travel times and times calculated assuming a Layer 2 velocity of 4.8 km/s and regional topography (Figure 7). These residuals can be explained by small-scale basement topography not seen on the profiling record. Basement terrain is much rougher perpendicular to the spreading axis (E-W) than parallel to it (N-S). The error bars in the upper-right corner represent 0.02 s, which is the estimated maximum error in the travel times. The smoothness of the curves indicates that the actual error may be somewhat less than this. The star (*) shows the depth to basement at Hole 417A. All lines pass through the origin by definition. The residuals for the south lines may be in poor agreement because the two tracks are not coincident (Figure 1-A).*

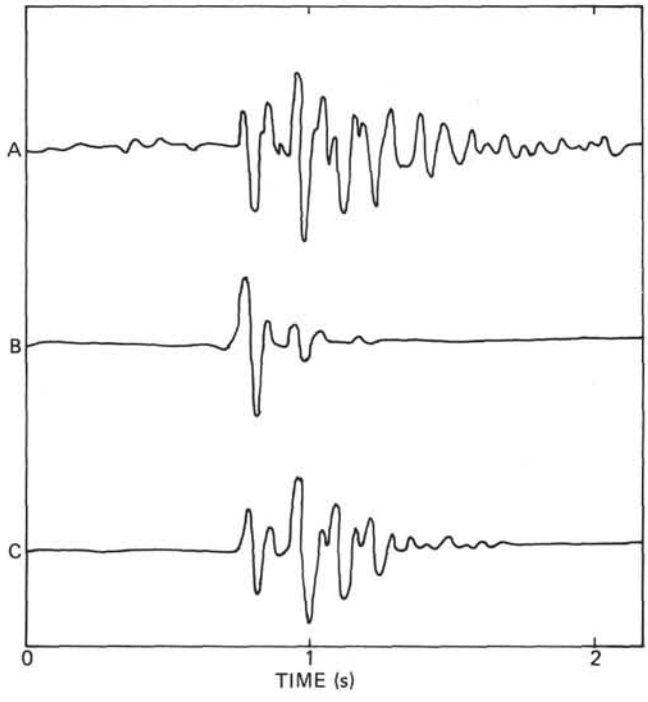

Figure 10. *Comparison of source wavelets for synthetics. Wavelet A is a typical seismogram for a near normal incidence arrival; wavelet B is the theoretical explosion wavelet; and wavelet C is the empirically selected source wavelet.*

3) There is too much energy within 0.5 s of the first arrival at long ranges (Region D). This appears to be an interference effect between the reflected and refracted arrivals from the 6.2 km/s layer (see Figure 8).

4) The S-wave energy does not drop around 9.5 km (Region C). Interference effects between all five ray paths (the direct path and reflected and refracted paths from each of the 6.2 km/s and 6.8 km/s layers) may cause the amplitude behavior here (see Figure 8).

5) The S-wave amplitudes in the critical region (7.0 to 8.0 km) are too weak (Region B).

Braile and Smith (1975) show that compressional wave amplitudes in a critical region (e.g., Region A) can be increased by replacing a first-order discontinuity with a gradient. They also demonstrate that a low amplitude head wave (e.g., Region E) can be produced by introducing a negative velocity gradient below the interface. A gradient model based on the step model of Figure 11 therefore was tried. Shear wave velocities were kept proportional to compressional wave velocities. Figure 12 shows a horizontal component synthetic seismogram with the steps in the first model replaced by gradients and a slight velocity decrease in Layer 3. Strong arrivals are present in the critical regions for both P and S waves. The Layer 3 refraction drops in amplitude around 9 km and there is a fairly wide band of low amplitude shear energy between 8.0 and 10.0 km. There is still, however, too much energy behind the first P arrivals at large ranges. Since this region is affected by the reflected and refracted arrivals from the 6.2 km/s layer (Figure 8), the next reasonable guess is to eliminate the layer as a separate entity.

If the two gradients in Layer 2 are replaced by a single gradient (Figure 13) the synthetic seismogram improves. The later P-energy is considerably reduced. The synthetic seismogram analysis does not support the presence of a distinct 6.2 km/s layer.

An attempt to make any more than a general analysis would be unwise. Comparison of seismograms for all the lines (Appendix A) shows significant variation in amplitude patterns within ranges of a kilometer or so, even for lines in the same direction. This behavior may be simply a result of inadequate coupling between the geophone and the rock. Alternatively, the effects of varying shot signal, unknown basement topography, lateral variations (possibly in the mid-sediment reflector), and inhomogeneities may be too complex to model adequately by conventional means. Amplitudes will be particularly sensitive to interference effects at ranges where more than one ray path arrives at the same time (e.g., the strong P-wave arrivals between 6 and 7 km on the south, east, and west lines).

The velocity decrease in Layer 3, which is necessary to make the refraction die away after 9 km, may be a local effect. Although the decrease in amplitude is observed on all the lines (Appendix A), it is contrary to most refraction experience and occurs in a region of poor signal-to-noise ratio along lines which are not long enough to define the phenomenon completely.

The higher velocities at the bottom of Layer 2 are consistent with Houtz and Ewing's (1976) results except that their evidence is from refracted arrivals while ours is from wide-angle reflection arrivals. The preference for gradients rather than steps concurs with work of Whitmarsh (1978) and Kennett and Orcutt (1976). The thickness of Layer 2 (1.34 km) is just within one standard deviation of the mean for crust of this age (1.74 $\pm$0.41, Houtz and Ewing, 1976) and is not unreasonable.

Figure 14 provides relative amplitude-distance plots of the first P- and S-wave arrivals for the four lines shot with the geophone at 6060 meters. At ranges less than 5 km, it is difficult to differentiate between P- and S-wave phases. Consequently, these data apply mostly to critically refracted and wide-angle reflected arrivals. Superimposed on the plots is the corresponding curve for the synthetic seismogram based on the two-stage gradient model (Figure 12). The compressional wave amplitude curves for the real data vary considerably and there are no significant differences between the north-south and east-west lines. Shear wave behavior is more stable. The east and north line P amplitudes are similar; the south line amplitudes are strongest; and the west line amplitudes are weakest. These trends do not correspond to the velocity trends mentioned above.

Variations in source signal were checked by looking at the sea bottom reflection on the shallow hydrophone (Appendix A). The reflection coefficient is approximately constant for sub-critical reflections for a water-solid interface (Grant and West, 1965). The amplitudes of the reflected arrivals are generally stable with extremes varying by a factor of about 2 from the mean. None of these extremes

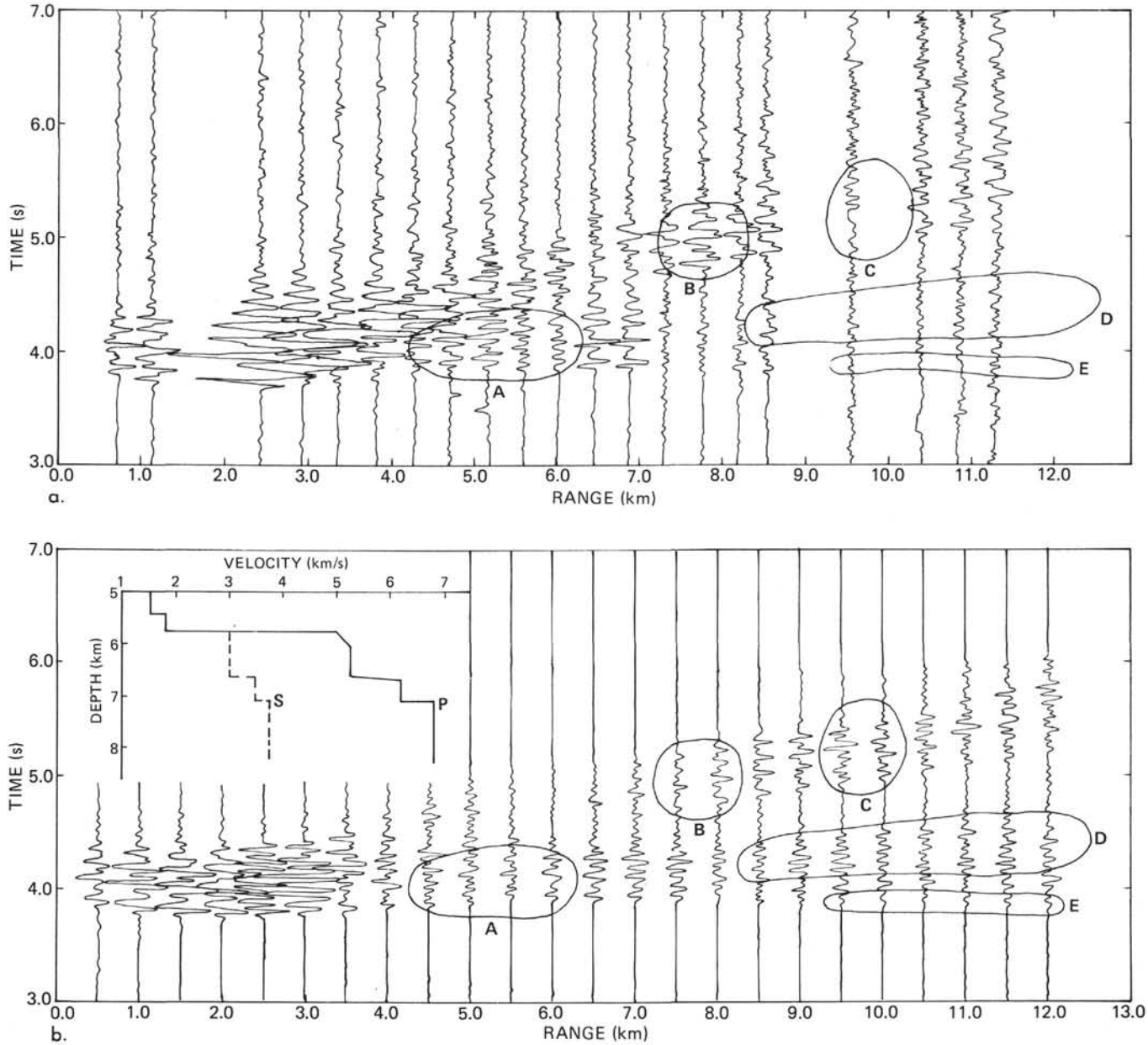

Figure 11. *Horizontal component synthetic seismogram analysis for the initial model using an empirical source: (a) is the observed horizontal component seismogram for the south line at the deep geophone position; (b) is the synthetic seismogram for the initial model. Model amplitudes in regions A and B are too small and in regions C, D, and E are too large. The regions and typical amplitudes in the regions were chosen by considering all the deep geophone position seismograms (Appendix A). Reduction velocity and amplitude weighting are the same on the two sections. Amplitude-distance plots for the four deep geophone lines are shown in Figure 14.*

corresponds to the significant peaks and troughs of the geophone amplitude-distance curves.

CONCLUSIONS

Lateral Velocity Variations

There is no point in looking for lateral velocity variations in Layer 2 unless the basement topography is known in detail. In the area surrounding Site 417, the profiling was inadequate because of the deep water which spoiled resolution and because of the strong mid-sediment reflector which masked deeper energy. These factors are also mentioned in Houtz and Ewing (1976).

Travel-time residuals from the OSE indicate that the basement topography is much rougher perpendicular to the magnetic lineations than parallel to them. The features perpendicular to the spreading direction are on the order of 0.20 km high and 2 km wide. They have the same dimensions as the volcanic relief observed in the FAMOUS area (Macdonald and Luyendyk, 1977).

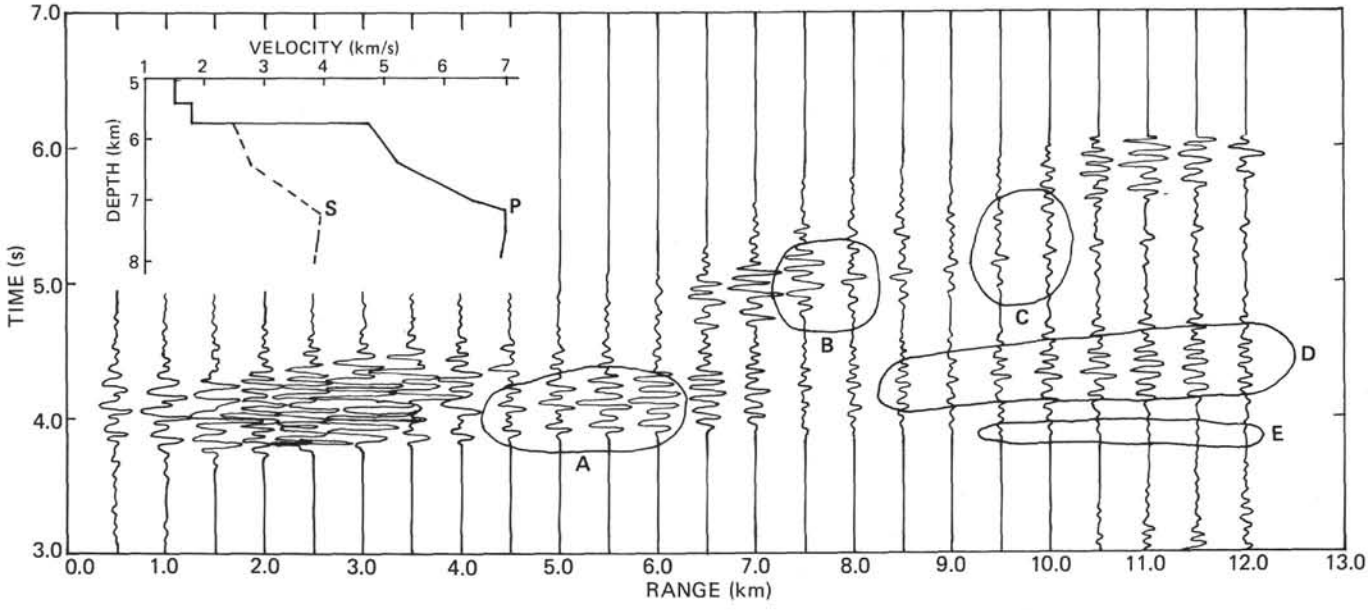

Figure 12. *Horizontal component synthetic seismogram for a model with gradients rather than steps. Amplitudes in Region D are still too large. Reduction velocity and amplitude weighting are the same as for the observed sections. The noise at 3 s between 10 and 12 km is the result of aliasing in the Fourier transform and is not significant.*

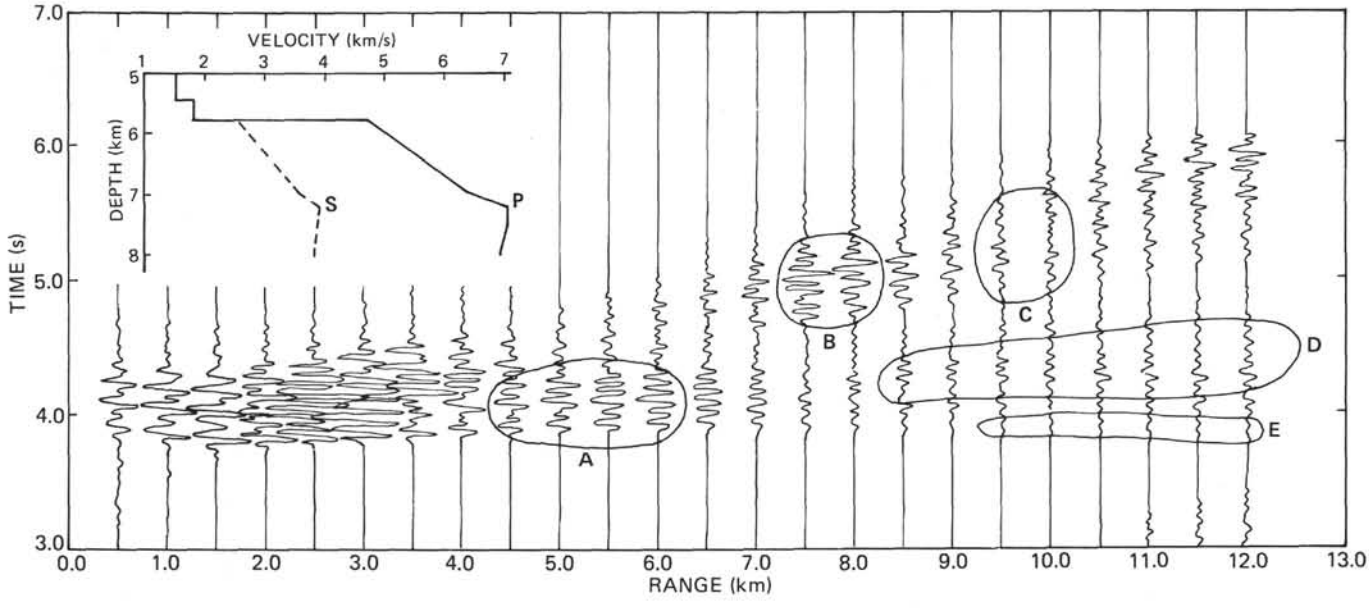

Figure 13. *Horizontal component synthetic seismogram for a model with a constant gradient in Layer 2. The amplitude pattern matches the observed pattern for the south line (Figure 11a) satisfactorily. Reduction velocity and amplitude weighting is the same as for the observed data sections. The noise at 3 s at long ranges (10 to 12 km) is the result of aliasing in the Fourier transform and is not significant.*

Pores, Vugs, and Fissures

The compressional wave velocity model for Layer 2 which best explains the OSE data at Site 417 is a uniform gradient from 4.8 km/s at the top of the basement to 6.4 km/s at 1.3 km depth. The corresponding S-wave velocities are 2.6 to 3.6 km/s. Since matrix P- and S-wave velocities for basalts are about 6.2 km/s and 3.3 km/s respectively, (Hamano, personal communication), the observations are consistent with the theory that cracks are closing with depth in Layer 2. The relationship between laboratory, OSE, and logging measurements is discussed in more detail by Salisbury et al. (this volume).

Anisotropy

No undisputed evidence for preferential crack orientation was found from either velocity or amplitude studies.

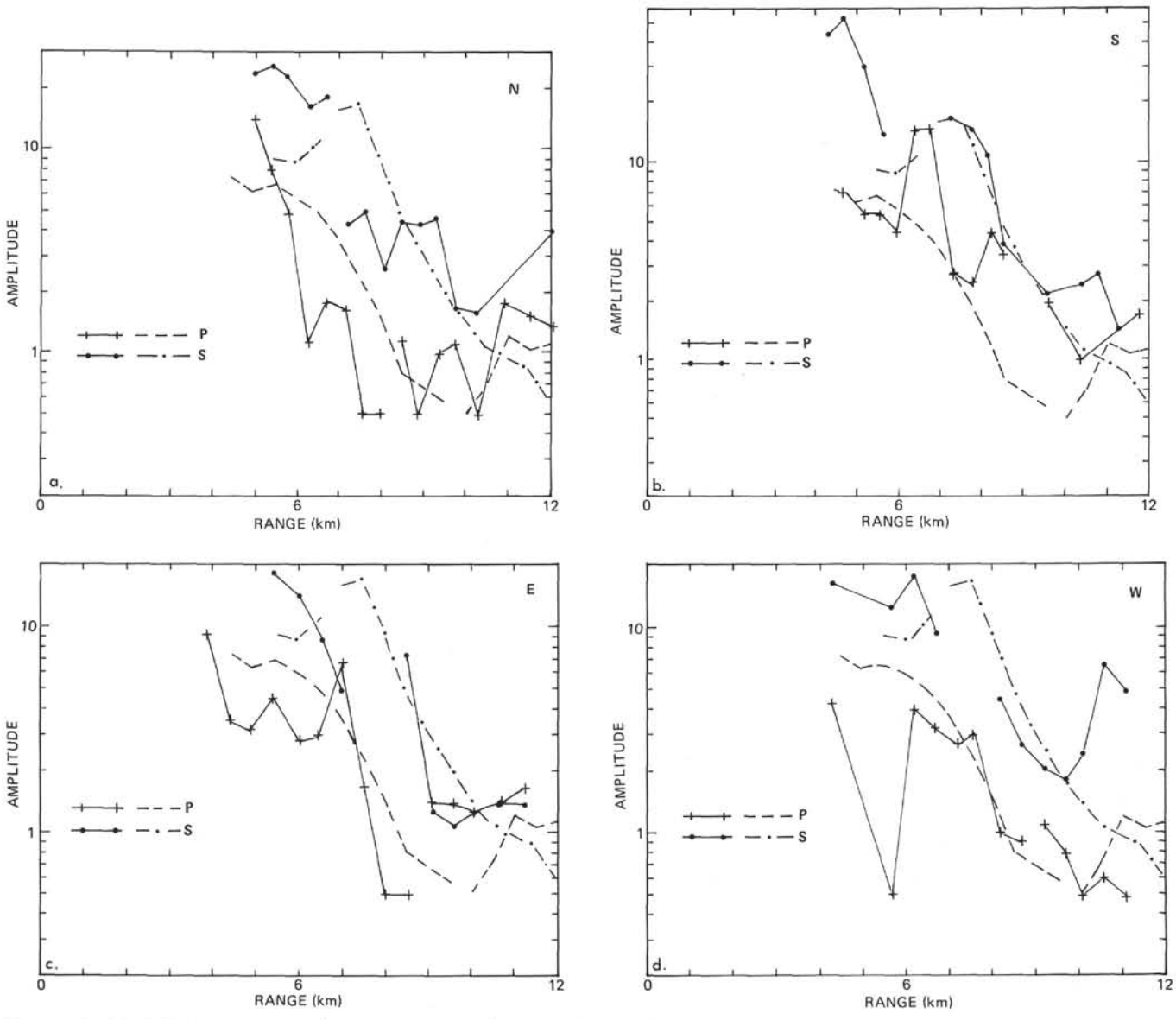

Figure 14. *(a-d) Relative amplitude-distance curves for lines shot to the deep geophone position. North, south, east, and west lines are represented by Figures a, b, c, and d, respectively. Amplitudes are the root mean square peak-to-peak amplitudes, in arbitrary units, of all three components (two components for synthetics). Solid lines are the curves for the observed data and the dashed lines are curves for the synthetic seismogram of Figure 12. The left P-wave segment corresponds to refracted P-wave arrivals from Layer 3 and the right P-wave segment corresponds to wide-angle reflected arrivals. The left S-wave segment corresponds to direct S-wave energy and the right segment to refracted energy from Layer 3. General trends have been modeled adequately but the observed amplitude data are not consistent or smooth enough to consider either more detailed structures or attenuation.*

Rugged basement topography introduces errors into the travel times on the order of ±0.05 s, which make accurate velocity determinations over short ranges impossible.

In general, shear waves are better for looking at anisotropy because the direct wave arrival is a straight line for about 3 km before it is confused with refractions and reflections (Figure 8). The compressional wave direct arrivals fall on a curve which is insensitive to velocity. The direct shear wave amplitude increases with range in contrast to direct compressional wave amplitude which decreases (Ergin, 1952). Also, shear wave anisotropy is theoretically greater than compressional wave anisotropy for water-filled cracks (Anderson et al., 1974). Unfortunately, shear waves arrive later in the record and are interfered with by late compressional wave energy.

If the large fissures observed at the Mid-Atlantic Ridge persist in old crust, the OSE should be able to detect an anisotropy of 0.2 km/s. The mean north-south shear wave velocity (2.56 ±0.04 km/s), however, is not significantly different from the mean east-west velocity (2.66 ±0.11 km/s). The east-west velocity is higher, contrary to what would be expected for oriented north-south cracks. The

fissures may be associated with layer 2A (Houtz and Ewing, 1976) which gradually thins out at about 40 m.y.B.P. If so, we would not expect to see anisotropy caused by fissures at Site 417 where the age is about 110 m.y.B.P. The OSE results are perfectly consistent with this theory: fissures close with age and cracks close with depth.

It is not clear why the fissures close with age. Certainly considerable secondary mineralization has occurred in the older rocks. Cores from Sites 417 and 418 show that voids and cracks are filled with calcite, smectite, zeolites, quartz, pyrite, and other alteration products (Sites 417 and 418, Site Reports, this volume). This mineralization was not as extensive in the younger crust cored on Leg 37 (Robinson, Hall, et al., 1977). Recovery rates in the younger crust were also much lower than in old crust (20% versus 70%), indicating either more voids, poorer consolidation, or both. The large fissures may fill with cemented breccia while the cracks stay open. Alternatively, large fissures may never have formed in the section of older crust examined here.

Average Layer 3 refracted P-wave velocities are 6.71 $\pm$0.30 km/s for north-south lines and 6.61 $\pm$0.41 km/s for east-west lines. The refracted S-wave velocities are 3.77 $\pm$0.10 km/s for north-south lines and 3.60 $\pm$0.09 km/s for east-west lines. These values are not convincing evidence for anisotropy in Layer 3. If, however, we assume that most of the spread in the errors is caused by small-scale topography and accept the mean values, then anisotropy on the order of 0.2 km/s may exist. Since the velocity gradients at the site indicate that the cracks on all scales are almost completely closed at the bottom of Layer 2, the anisotropy could be related to crystal orientation or residual fabric (Christensen, 1972; Friedman and Bur, 1974).

The OSE should be performed in younger crust where Layer 2A exists in an attempt to detect preferred crack orientation and its extent with depth. The anisotropy should be large enough to see above the topographic effects. The OSE is more suitable for this purpose than conventional refraction with either sea-bottom or surface receivers because Layer 2A is frequently a poor refractor and when refracted arrivals are present, they appear over only a short distance making accurate velocity determinations difficult (Houtz and Ewing, 1976).

Attenuation

Because of the shallow depth of the geophone (228 m in basement), no determination of attenuation from short-range (vertical incidence) shots could be made. The effects of attenuation on long-range shots are much less than the observed amplitude variations which could be caused by inadequate clamping, undetermined basement topography, or lateral inhomogeneities.

ACKNOWLEDGMENTS

We would like to thank Dr. J. Heirtzler, Dr. H. Stewart, Jr., Dr. S. White, Dr. W. Bryan, Dr. P. Robinson, Mr. R. Knapp, Mr. V. Larsen, the drilling personnel of *Glomar Challenger* for Leg 52, the DSDP marine technicians, Captain Clarke and the crew of the *Glomar Challenger*, Captain Neill and the crew of the *Virginia Key* for their co-operation in organizing and running the Oblique Seismic Experiment. Dr. G. M. Purdy, Mr. T. Stetson, and Mr. J. Broda helped bridge trans-Atlantic communications difficulties and arranged for the explosives. We would also like to thank Drs. Townsend and Mumford at the Cavendish Laboratory for making their digitizing equipment available, and Andrew Bunch for his digital data reduction programs.

The *Glomar Challenger* ship time was provided by the Deep Sea Drilling Project. The Natural Environment Research council funded the other field work and development. The University of Cambridge computing service supplied computer time for the data reduction. We would like to thank Shell Canada Ltd. for supporting Stephen's personal expenses for three and a half years. Drs. B.L.N. Kennett and R.S. White from the Department of Geodesy and Geophysics, Madingley Rise, Madingley Road Cambridge, U.K., kindly reviewed the paper.

REFERENCES

Anderson, D.L., Minster, B., and Cole, D., 1974. The effect of oriented cracks on seismic velocities, *J. Geophys. Res.*, v. 79, p. 4011-4016.

Ballard, R.D. and van Andel, T.H., 1977. Morphology and tectonics of the inner rift valley at lat 36°50′N on the Mid-Atlantic Ridge, *Bull. Geol. Soc. Am.*, v. 88, p. 507-530.

Ballard, R.D., Bryan, W.B., Heirtzler, J.R., Keller, G., Moore, J.G., and van Andel, T.H., 1975. Manned submersible operations in the Famous area: Mid-Atlantic Ridge, *Science*, v. 190, p. 103-108.

Brace, W.F., Silver, E., Hadley, K., and Goetze, C., 1972. Cracks and pores: a closer look, *Science*, v. 178, p. 162.

Braile, L.W. and Smith, R.B., 1975. Guide to the interpretation of crustal refraction profiles, *Geophys. J. Roy. Astron. Soc.*, v. 40, p. 145-176.

Christensen, N.I., 1972. Seismic anisotropy in the lower oceanic crust, *Nature*, v. 237, p. 450-451.

Ergin, K., 1952. Energy ratio of the seismic waves reflected and refracted at a rock-water boundary, *Bull. Seismol. Soc. Am.*, v. 42, p. 342-372.

Fowler, C.M.R., 1976a. Seismic studies of the Mid-Atlantic Ridge, Ph.D. thesis, Department of Geodesy and Geophysics, University of Cambridge, Cambridge, U.K.

———, 1976b. Crustal structure of the Mid-Atlantic Ridge crest at 37°N, *Geophys. J. Roy. Astron. Soc.*, v. 47, p. 459-491.

Friedman, M. and Bur, T.R., 1974. Investigations of the relations among residual strain, fabric, fracture and ultrasonic attenuation and velocity in rocks, *Internat. J. Rock Mech., Mineral Sci. Geomech.*, v. 11, p. 221-234.

Fuchs, K. and Müller, G., 1971. Computation of synthetic seismograms with the reflectivity method and comparison with observations, *Geophys. J. Roy. Astron. Soc.*, v. 23, p. 417-433.

Gal'perin, E.I., 1974. *Vertical seismic profiling:* Tulsa (Society of Exploration Geophysicists).

Geo Space Corporation, 1972. *Technical manual for the wall-lock well geophone:* Houston, Texas (Geo Space Corporation).

Gordon, R.B. and Nelson, C., 1966. Anelastic properties of the earth, *Rev. Geophys.*, v. 4, p. 457-477.

Grant, F.S., and West, G.F., 1965. *Interpretation theory in applied geophysics:* New York (McGraw-Hill).

Hamilton, E.L., 1976. Sound attenuation as a function of depth in the sea floor, *J. of the Acoustic Soc. of Am.*, v. 59, p. 528-535.

Hess, H., 1964. Seismic anisotropy of the uppermost mantle under oceans, *Nature*, v. 203, p. 629-631.

Houtz, R.E., 1976. Seismic properties of layer 2A in the Pacific, *J. Geophys. Res.*, v. 81, p. 629-631.

Houtz, R., and Ewing, J.I., 1976. Upper crustal structure as a function of plate age, *J. Geophys. Res.*, v. 81, p. 2490-2498.

Hyndman, R.D., 1977. Seismic velocity measurements of basement rocks from DSDP Leg 37. *In* Aumento, F., Melson, W.G., et al. *Initial Reports of the Deep Sea Drilling Project,* v. 37: Washington (U.S. Government Printing Office), p. 373-387.

Hyndman, R.D., Von Herzen, R.P., Erickson, A.J., and Jolivet, J., 1977. Heat flow measurements, DSDP Leg 37. *In* Aumento, F., Melson. W.G., et al., *Initial Reports of the Deep Sea Drilling Project,* v. 37: Washington (U.S. Government Printing Office), p. 347-362.

Jackson, D.D. and Anderson, D.L., 1970. Physical mechanisms of seismic attenuation, *Rev. Geophys. Space Phys.,* v. 8, p. 1-63.

Kennett, B.L.N., 1975. The effect of attenuation on seismograms. *Bull. Seismol. Soc. Am.,* v. 65, p. 1643-1651.

Kennett, B.L.N. and Orcutt, J.A., 1976. A comparison of travel time inversions for marine refraction profiles, *J. Geophys. Res.,* v. 81, p. 4061-4070.

Laughton, A.S., 1963. Microtopography. *In* Hill, M.N. (Ed.), *The sea:* New York (Interscience), v. 3, p. 437.

Laughton, A.S., Hill, M.N., and Allan, T.D., 1960. Geophysical investigations of a seamount 150 miles north of Madeira, *Deep-Sea Res.,* v. 7, p. 117-141.

Lister, C.R.B., 1974. Water percolation in the oceanic crust, *Trans. Am. Geophys. Union,* v. 55, p. 740-742.

Lort, J.M. and Matthews, D.H., 1972. Seismic velocities measured in rocks of the Troodos igneous complex, *Geophys. J. Roy. Astron. Soc.,* v. 27, p. 383-392.

Ludwig, W.J., Nafe, J.E., and Drake, C.K., 1970. Seismic refraction. *In* Maxwell, A.E. (Ed.), *The sea:* New York (Interscience), v. 4, pt. 1, p. 53.

Luyendyk, B.P. and Macdonald, K.C., 1977. Physiography and structure of the inner floor of the Famous rift valley: observations with a deep-towed instrument package, *Bull. Geogr. Soc. Am.,* v. 88, p. 648-663.

Macdonald, K.C. and Luyendyk, B.P., 1977. Deep-tow studies of the structure of the Mid-Atlantic Ridge crest near lat. 37°N, *Bull. Geol. Soc. Am.,* v. 88, p. 621-636.

McDonnal, F.J., Angona, F.A., Mills, R.L., Sengbush, R.L., and Nostrand, R.G., and White, J.E., 1958. Attenuation of shear and compressional waves in Pierre shale, *Geophysics,* v. 23, p. 421-439.

Neprochnov, Y.P., 1971. Seismic studies of the crustal structure beneath the seas and oceans, *Oceanology* (English translation), v. 11, p. 709-715.

Neprochnov, Y.P., Neprochnova, A.F., Zverev, S.M., and Mironova, V.I., 1967. Deep seismic sounding of the earth's crust in the central part of the Black Sea depression. *In* Zverev, S.M. (Ed.), *Problems in deep seismic sounding:* New York (English Translations Consultants Bureau), p .44-78.

O'Brien, P.N.S. and Lucas, A.L., 1971. Velocity dispersion of seismic waves, *Geophys. Prospecting,* v. 19, p. 1-26.

Raitt, R.W., 1963. The crustal rocks. *In* Hill, M.N. (Ed.), *The sea:* New York (Interscience), v. 3, p. 85.

Robinson, P.T., Hall, J.M., Aumento, F., Melson, W.G., Bougault, H., Dmitriev, L., Fischer, J.F., Flower, M., Howe, R.C., Hyndman, R.D., Miles, G.A., and Wright, T.L, 1977. Leg 37 cruise synthesis: The lithology, structure, petrology, and magnetic history of layer 2. *In* Aumento, F., Melson, W.G., et al., *Initial Reports of the Deep Sea Drilling Project,* v. 37: Washington (U.S. Government Printing Office), p. 987-997.

Spiess, F.N. and Mudie, J.D., 1970. Small scale topographic and magnetic features. *In* Maxwell, A.E. (Ed.), *The sea:* New York (Interscience), v. 4, pt. 1, p. 205.

Stephen, R.A., 1977a. The Oblique Seismic Experiment in Oceanic Crust, Ph.D. Thesis, Department of Geodesy and Geophysics, Madingley Road, Cambridge, England.

———— , 1977b. Synthetic seismograms for the case of the receiver within the reflectivity zone, *Geophys. J. Roy. Astron. Soc.,* v. 51, p. 169-181.

White, J.E., 1965. *Seismic waves: radiation, transmission, and attenuation:* New York (McGraw-Hill Book Company), p. 143.

Whitmarsh, R.B., 1978. Seismic refraction studies of the upper igneous crust in the north Atlantic and porosity estimates for Layer 2, *Earth Planet. Sci. Lett.,* v. 37, p. 451-464.

APPENDIX A
LOCATION OF OBLIQUE SEISMIC DATA (OSE) SHOTS
(Figure A-1)

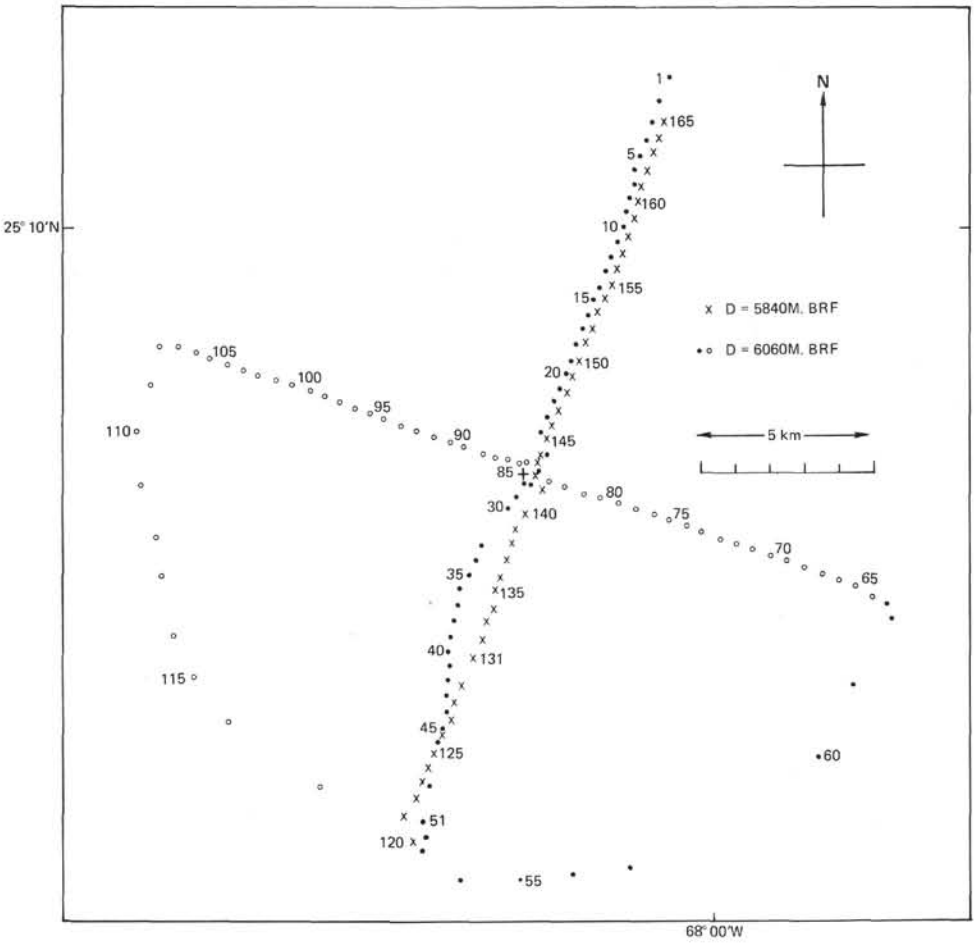

Figure A1. *Shot locations relative to* Glomar Challenger *(+). Ranges were computed from the direct water wave travel-time and bearings were monitored from* Glomar Challenger *during the experiment. The lines referred to in the text and Appendix B are defined as follows:*

Direction (m)	Shots
North (6060)	1-24
South (6060)	29-53
East (6060)	64-84
West (6060)	87-108
North (5840)	144-165
South (5840)	120-141
Southeast azimuths	53-63
Southwest azimuths	108-119

APPENDIX B
DATA COLLECTED ON THE OBLIQUE SEISMIC EXPERIMENT (OSE)

Figures B-1a to B-9c are shown on the following pages. Figures B-1a to B-6c are record sections of the three-component geophone data for the north, south, east, and west lines with the geophone at 6060 meters BRF and, for the north and south lines, with the geophone at 5840 meters. Figures B-7a to B-7f are the corresponding shallow hydrophone records; Figures B-8a to B-9c are the geophone records for the azimuthal shots.

All the geophone sections have the same weighting. That is, up to 7 km, no weighting has been performed; over 7 km, the amplitudes have been multiplied by $(\text{range}/7.0)^{2.9}$ Direct comparison of amplitudes can be made between sections. Traces on the hydrophone sections have been normalized individually. No terrain corrrections have been made on the sections.

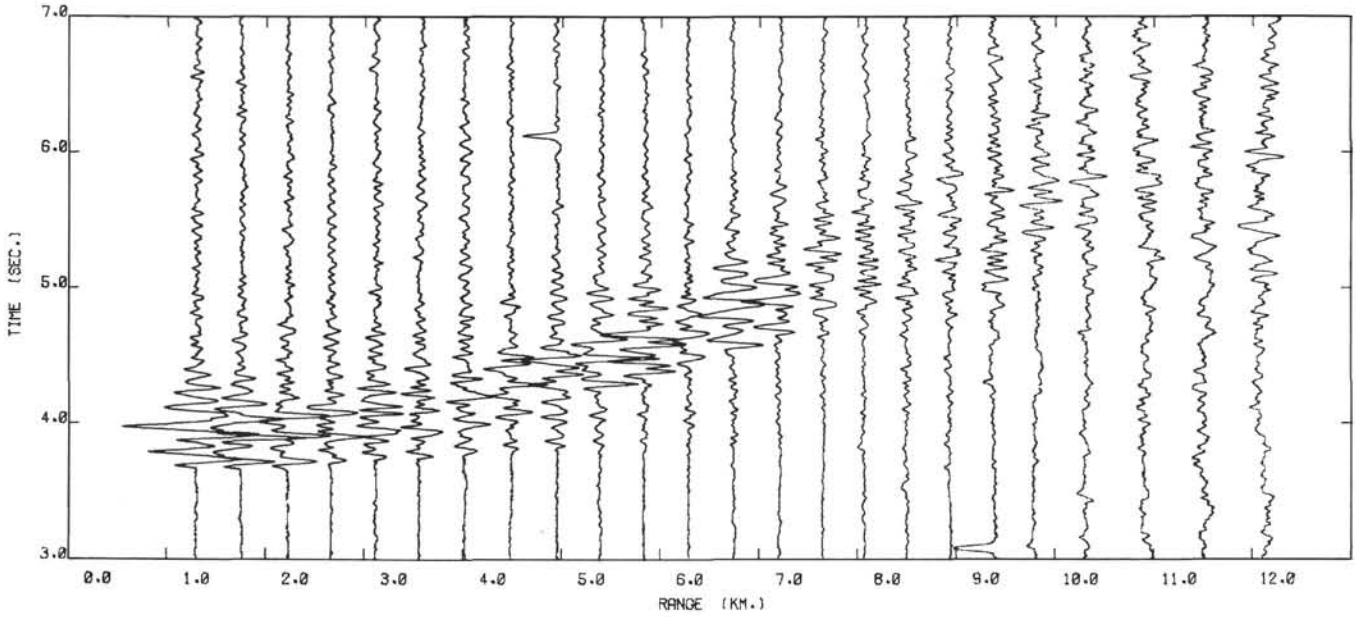

Figure B-1a

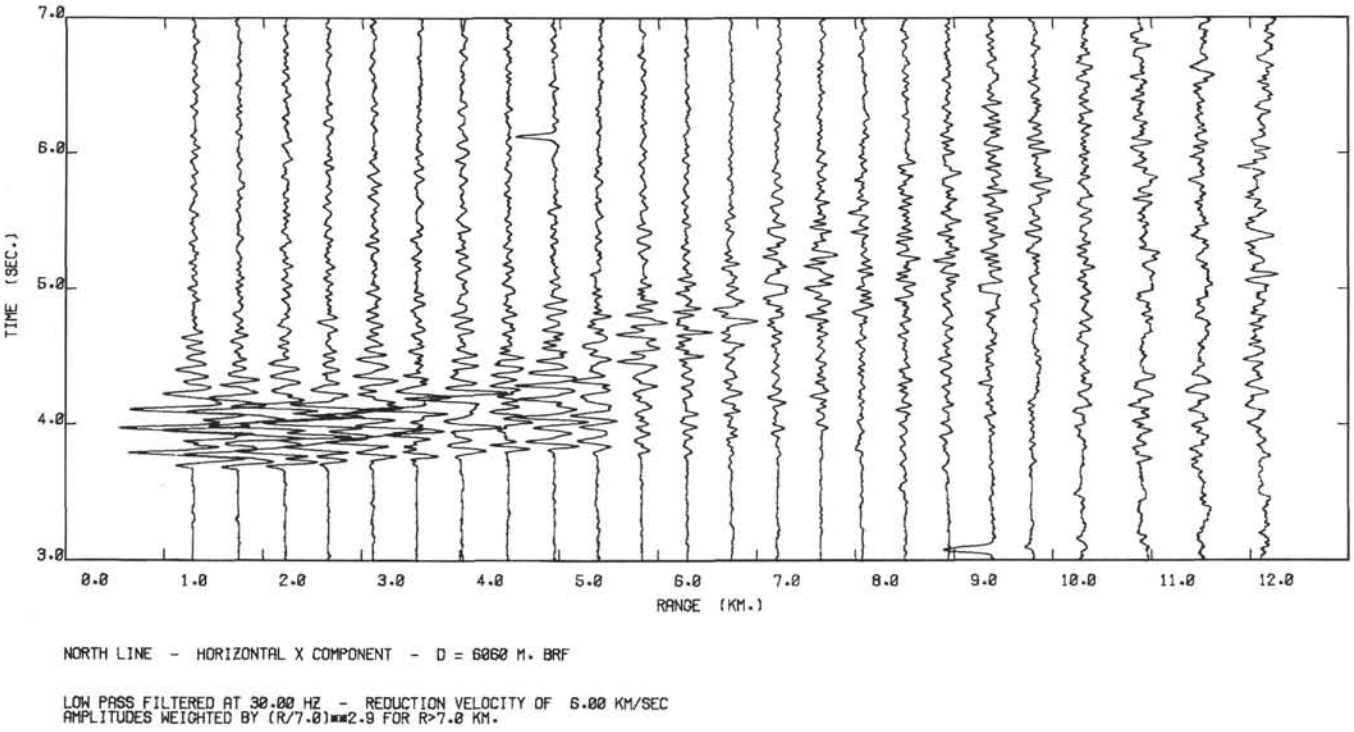

Figure B-1b

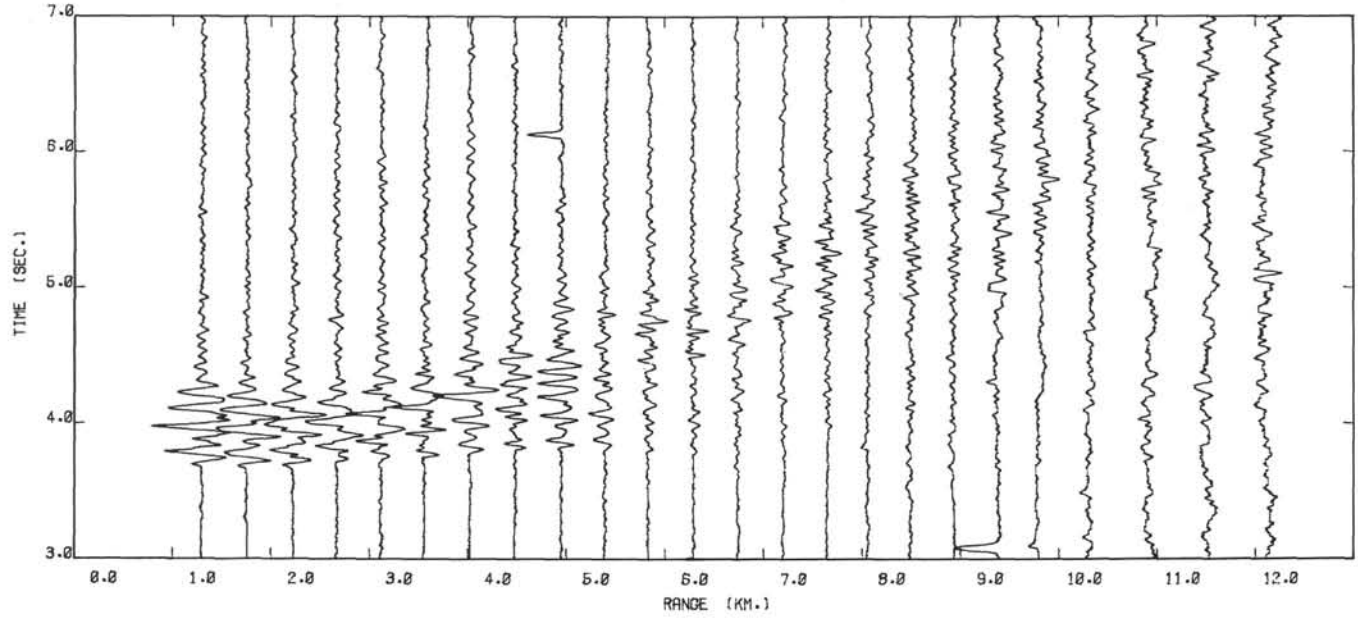

NORTH LINE - HORIZONTAL Y COMPONENT - D = 6060 M. BRF

LOW PASS FILTERED AT 30.00 HZ - REDUCTION VELOCITY OF 6.00 KM/SEC
AMPLITUDES WEIGHTED BY (R/7.0)**2.9 FOR R>7.0 KM.

Figure B-1c

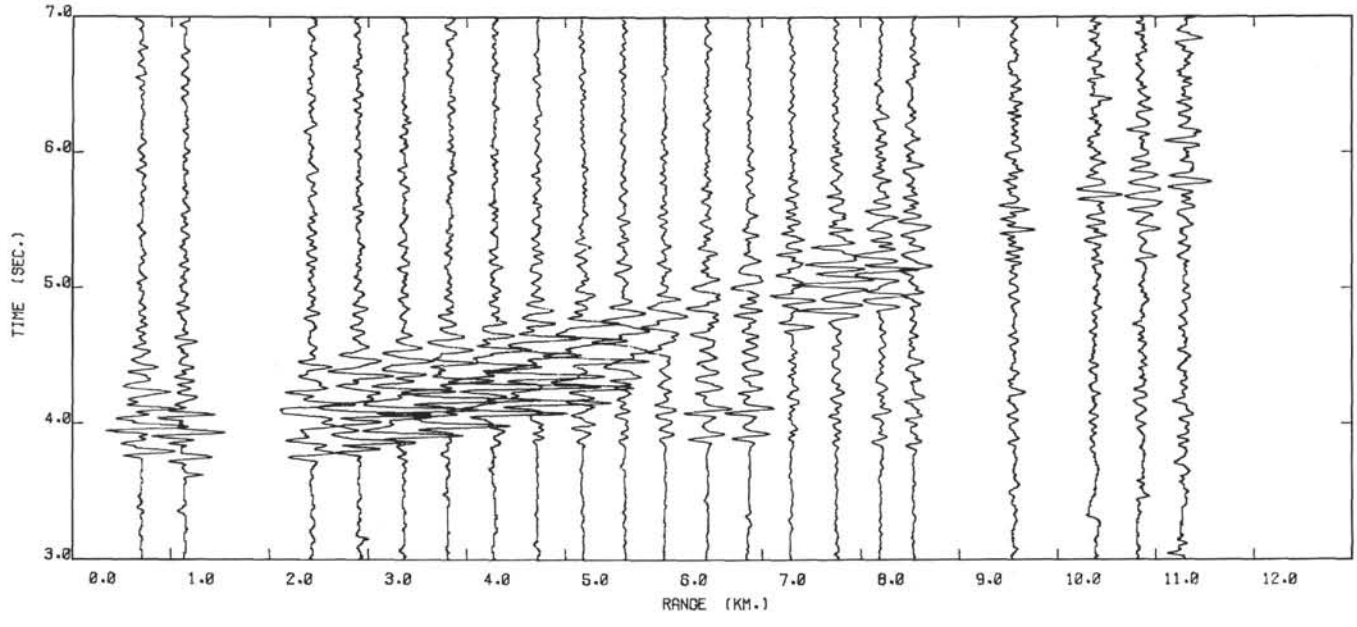

SOUTH LINE - VERTICAL COMPONENT - D = 6060 M. BRF

LOW PASS FILTERED AT 30.00 HZ - REDUCTION VELOCITY OF 6.00 KM/SEC
AMPLITUDES WEIGHTED BY (R/7.0)**2.9 FOR R>7.0 KM.

Figure B-2a

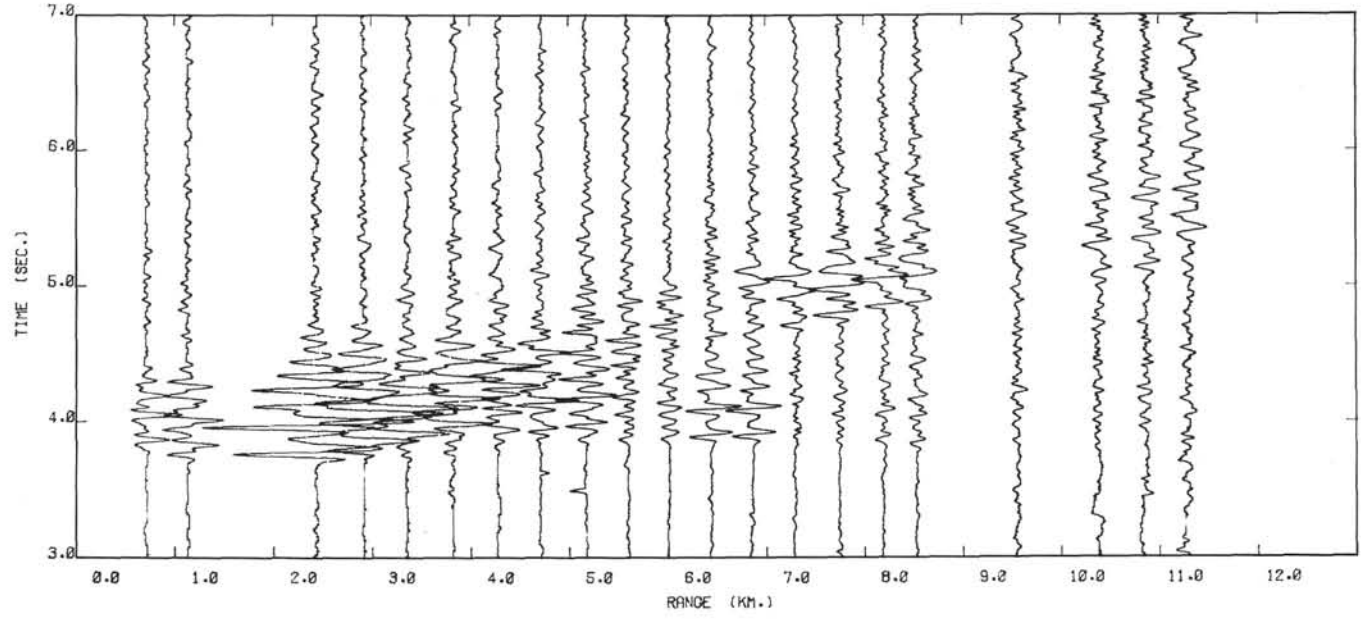

SOUTH LINE - HORIZONTAL X COMPONENT - D = 6060 M. BRF

LOW PASS FILTERED AT 30.00 HZ - REDUCTION VELOCITY OF 6.00 KM/SEC
AMPLITUDES WEIGHTED BY (R/7.0)**2.9 FOR R>7.0 KM.

Figure B-2b

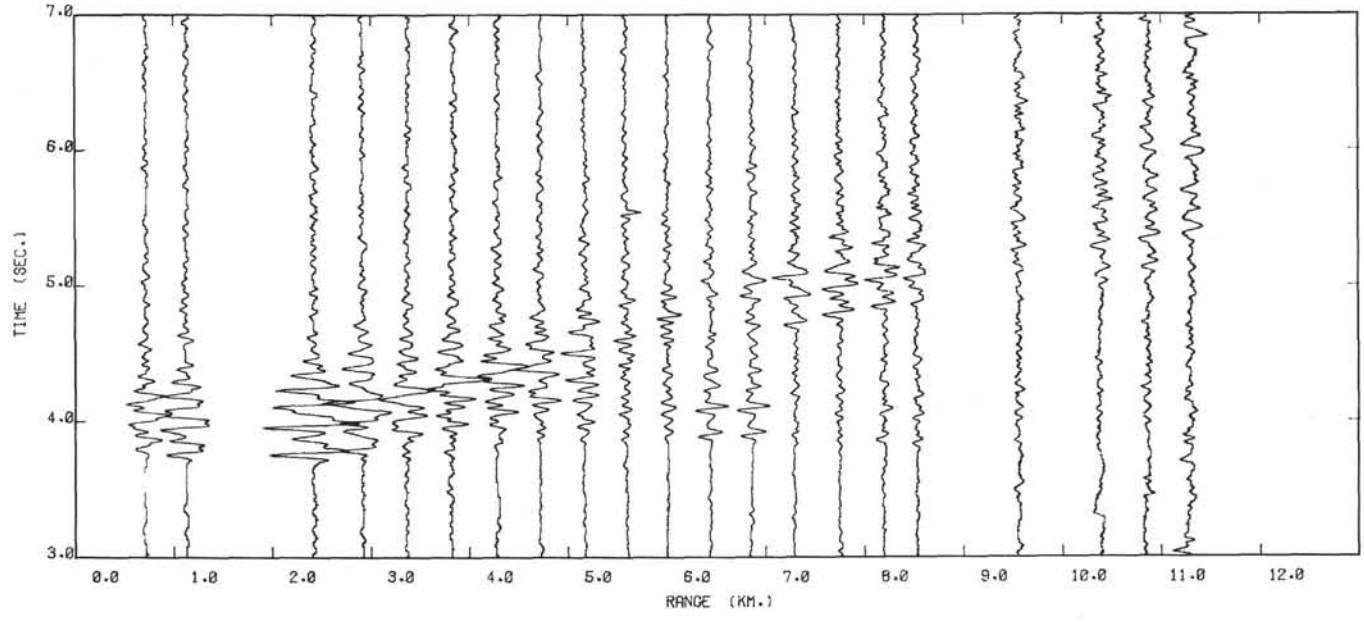

SOUTH LINE - HORIZONTAL Y COMPONENT - D = 6060 M. BRF

LOW PASS FILTERED AT 30.00 HZ - REDUCTION VELOCITY OF 6.00 KM/SEC
AMPLITUDES WEIGHTED BY (R/7.0)**2.9 FOR R>7.0 KM.

Figure B-2c

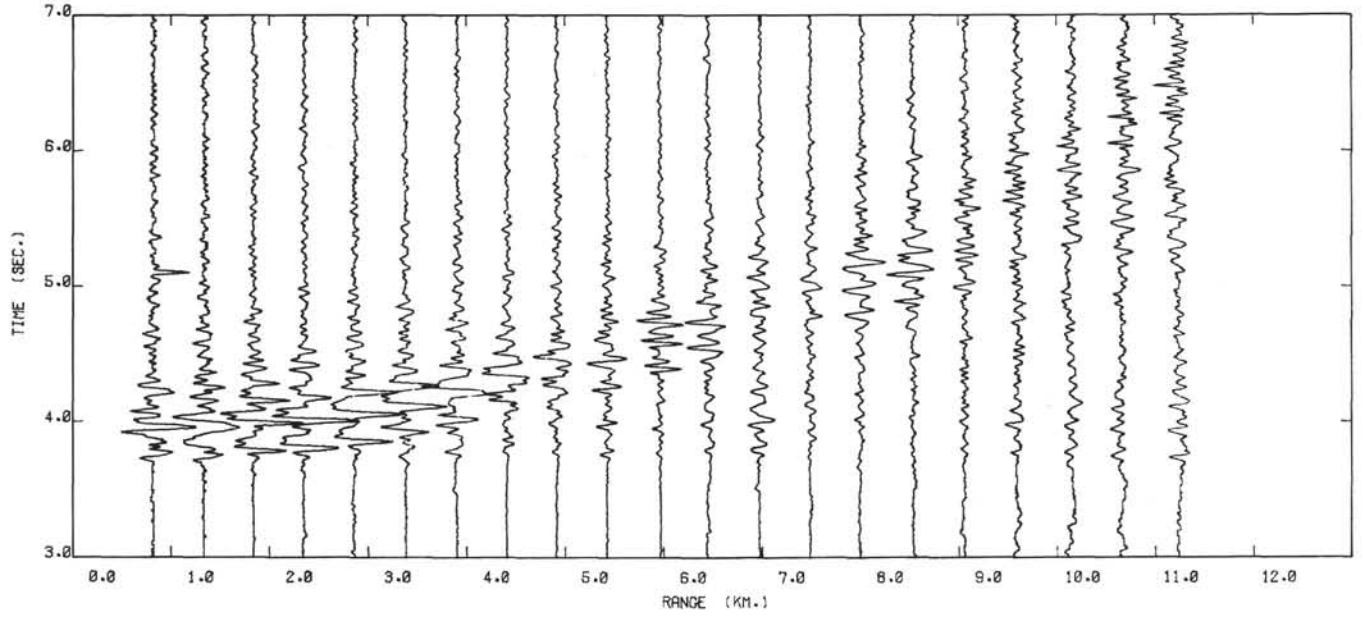

EAST LINE - VERTICAL COMPONENT - D = 6060 M. BRF

LOW PASS FILTERED AT 30.00 HZ - REDUCTION VELOCITY OF 6.00 KM/SEC
AMPLITUDES WEIGHTED BY (R/7.0)**2.9 FOR R>7.0 KM.

Figure B-3a

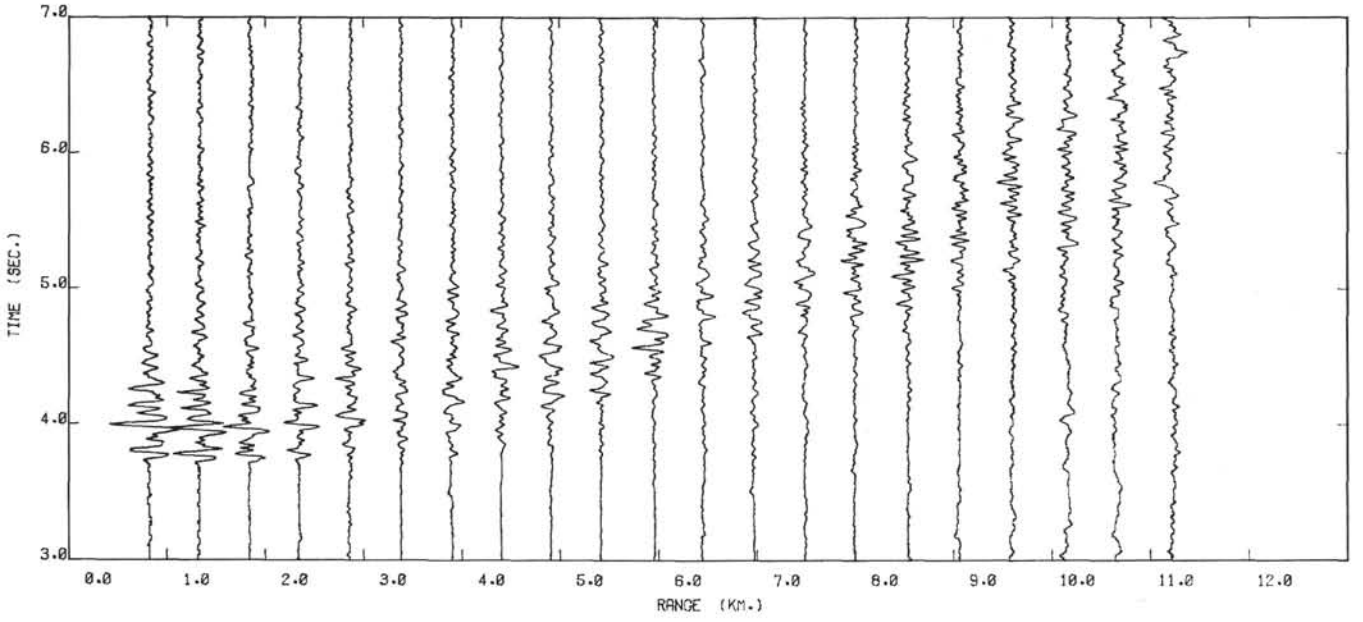

EAST LINE - HORIZONTAL X COMPONENT - D = 6060 M. BRF

LOW PASS FILTERED AT 30.00 HZ - REDUCTION VELOCITY OF 6.00 KM/SEC
AMPLITUDES WEIGHTED BY (R/7.0)**2.9 FOR R>7.0 KM.

Figure B-3b

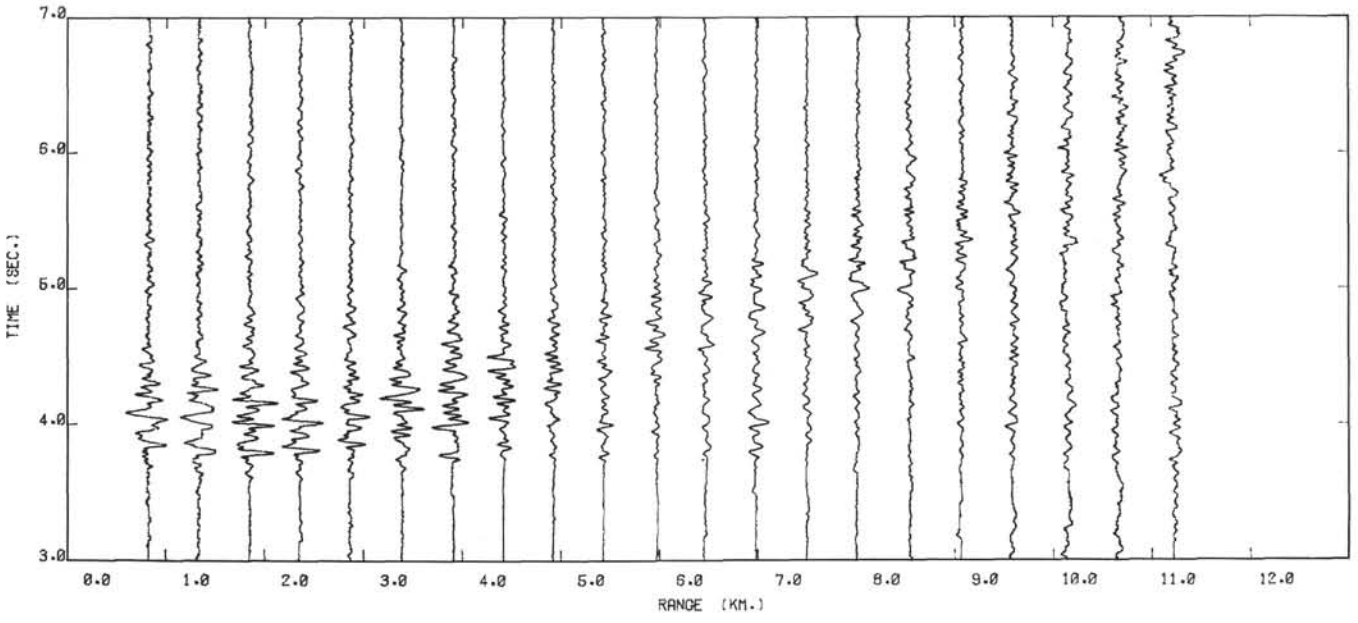

EAST LINE - HORIZONTAL Y COMPONENT - D = 6060 M. BRF

LOW PASS FILTERED AT 30.00 HZ - REDUCTION VELOCITY OF 6.00 KM/SEC
AMPLITUDES WEIGHTED BY (R/7.0)**2.9 FOR R>7.0 KM.

Figure B-3c

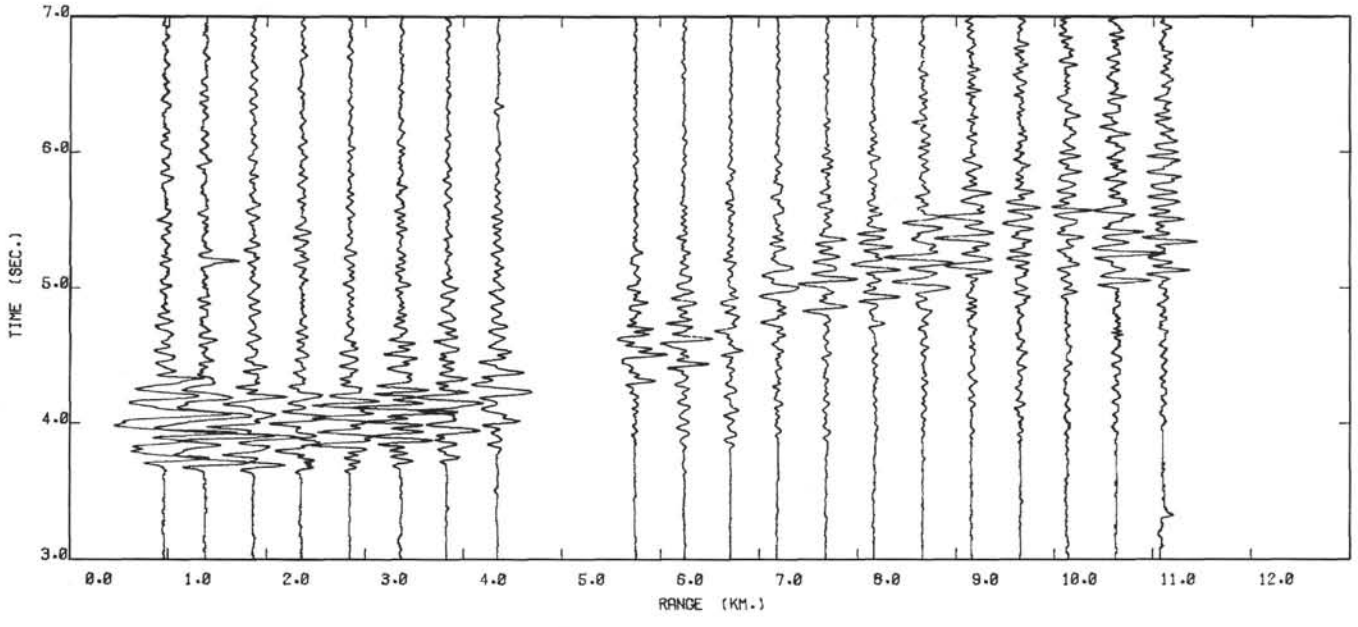

WEST LINE - VERTICAL COMPONENT - D = 6060 M. BRF

LOW PASS FILTERED AT 30.00 HZ - REDUCTION VELOCITY OF 6.00 KM/SEC
AMPLITUDES WEIGHTED BY (R/7.0)**2.9 FOR R>7.0 KM.

Figure B-4a

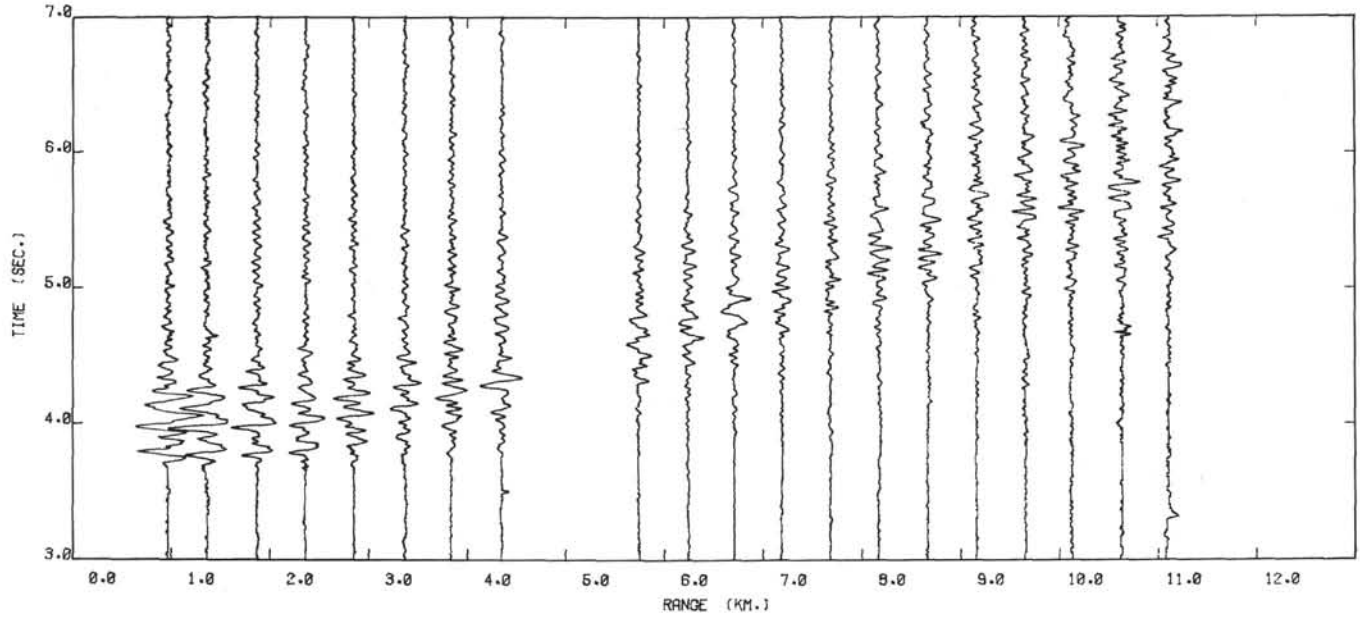

WEST LINE - HORIZONTAL X COMPONENT - D = 6060 M. BRF

LOW PASS FILTERED AT 30.00 HZ - REDUCTION VELOCITY OF 6.00 KM/SEC
AMPLITUDES WEIGHTED BY (R/7.0)**2.9 FOR R>7.0 KM.

Figure B-4b

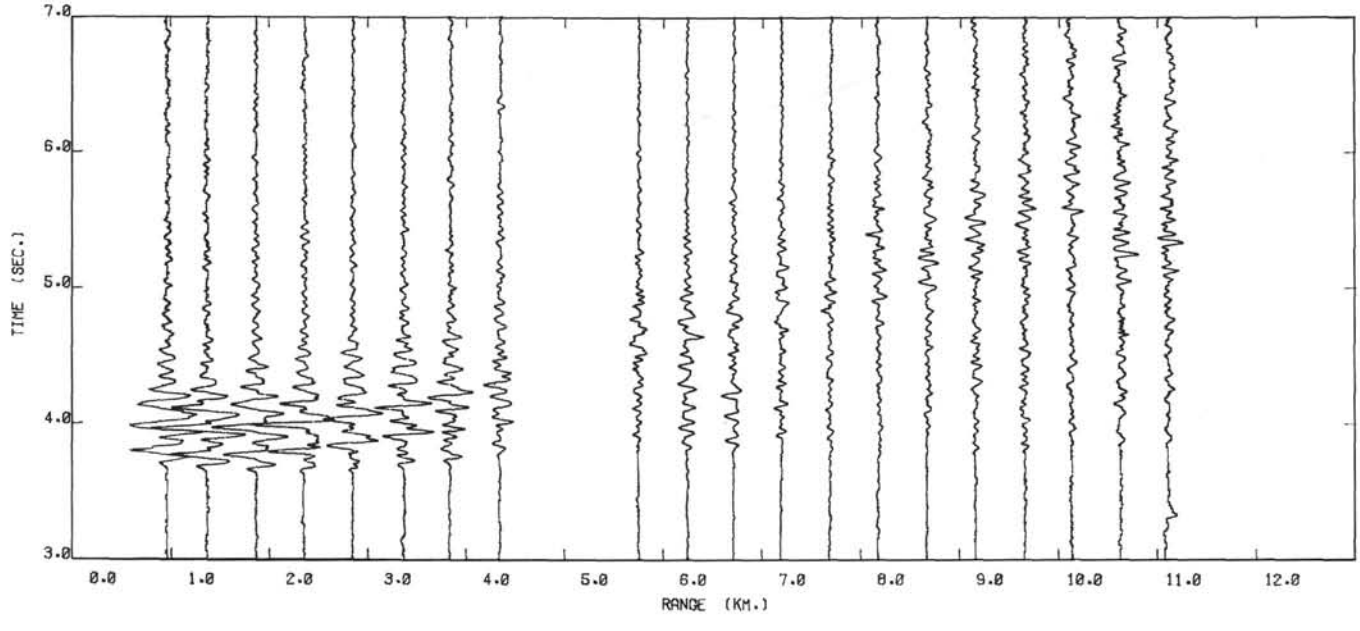

WEST LINE - HORIZONTAL Y COMPONENT - D = 6060 M. BRF

LOW PASS FILTERED AT 30.00 HZ - REDUCTION VELOCITY OF 6.00 KM/SEC
AMPLITUDES WEIGHTED BY (R/7.0)**2.9 FOR R>7.0 KM.

Figure B-4c

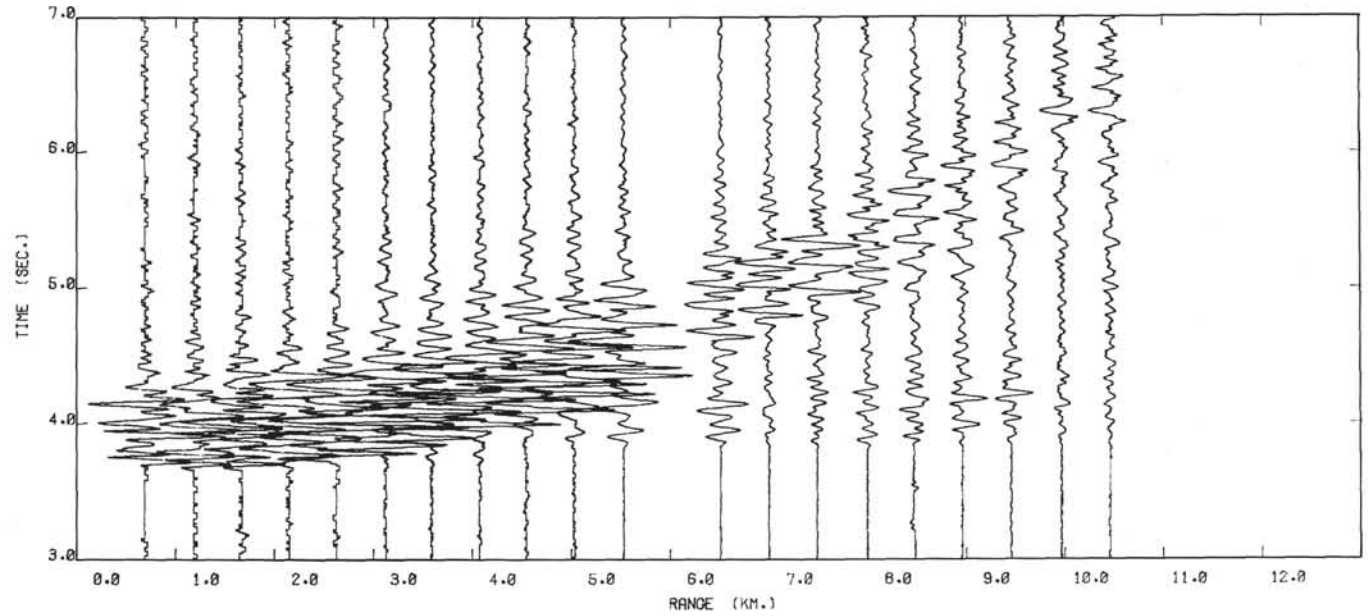

SOUTH LINE - VERTICAL COMPONENT - D = 5840 M. BRF

LOW PASS FILTERED AT 30.00 HZ - REDUCTION VELOCITY OF 6.00 KM/SEC
AMPLITUDES WEIGHTED BY (R/7.0)**2.9 FOR R>7.0 KM.

Figure B-5a

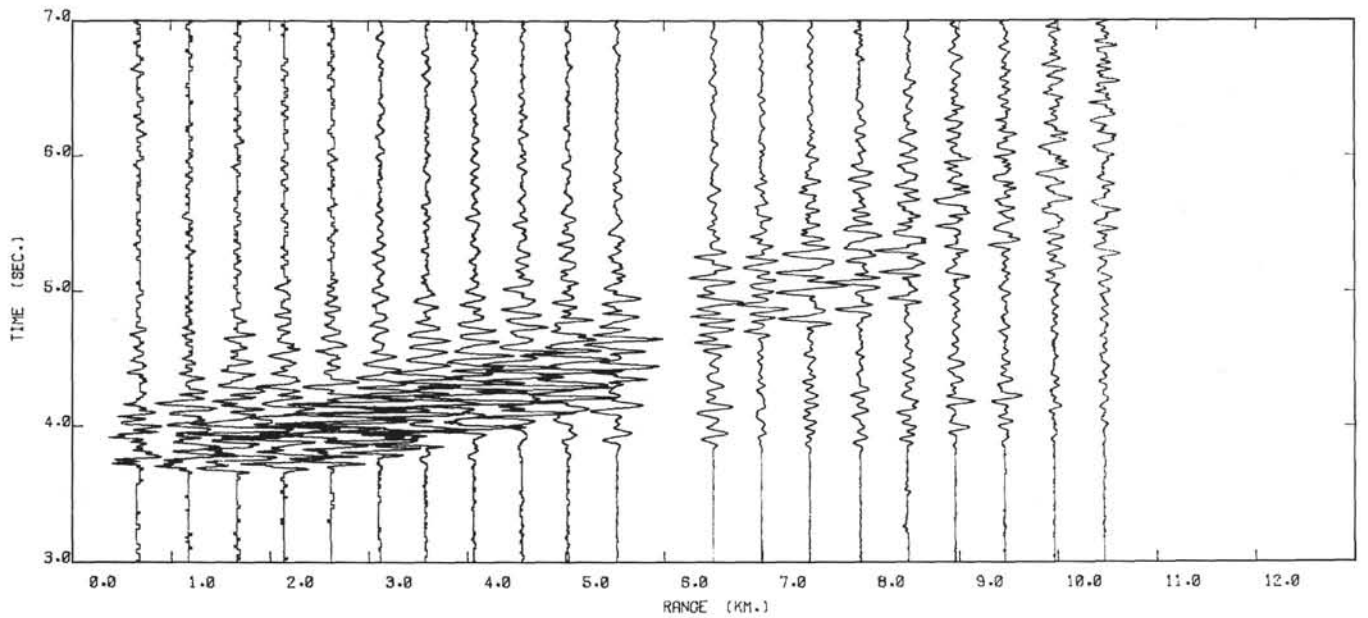

SOUTH LINE - HORIZONTAL X COMPONENT - D = 5840 M. BRF

LOW PASS FILTERED AT 30.00 HZ - REDUCTION VELOCITY OF 6.00 KM/SEC
AMPLITUDES WEIGHTED BY (R/7.0)**2.9 FOR R>7.0 KM.

Figure B-5b

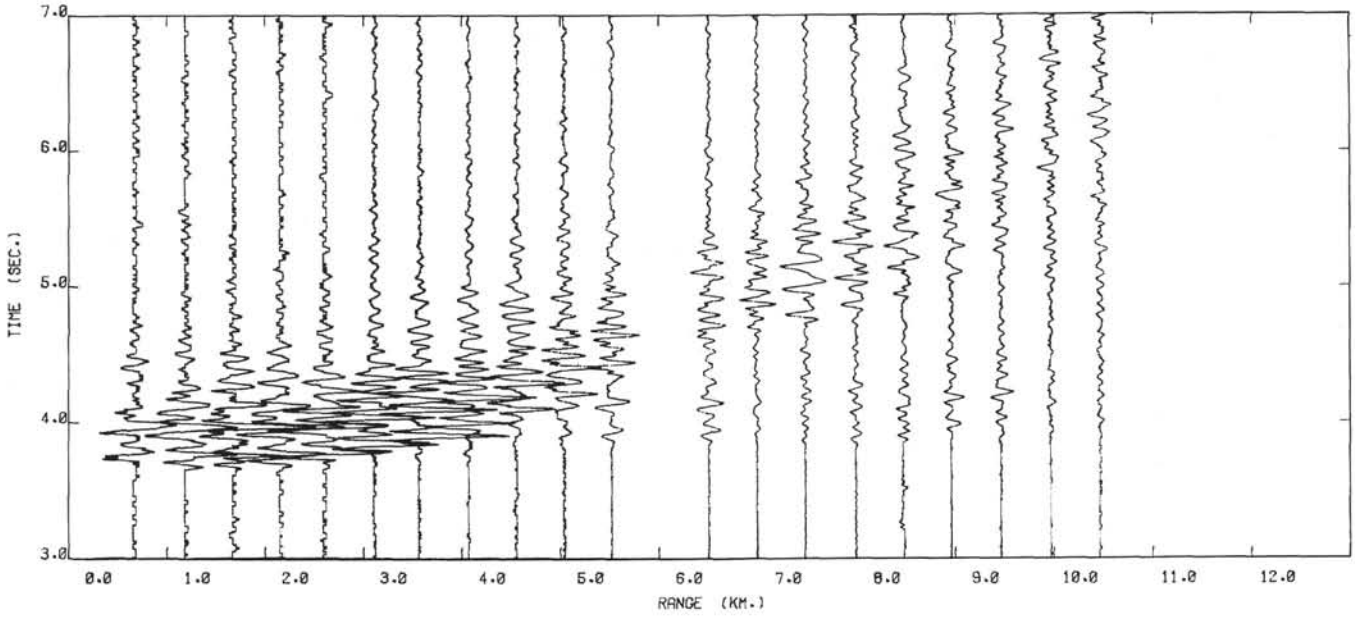

SOUTH LINE - HORIZONTAL Y COMPONENT - D = 5840 M. BRF

LOW PASS FILTERED AT 30.00 HZ - REDUCTION VELOCITY OF 6.00 KM/SEC
AMPLITUDES WEIGHTED BY (R/7.0)**2.9 FOR R>7.0 KM.

Figure B-5c

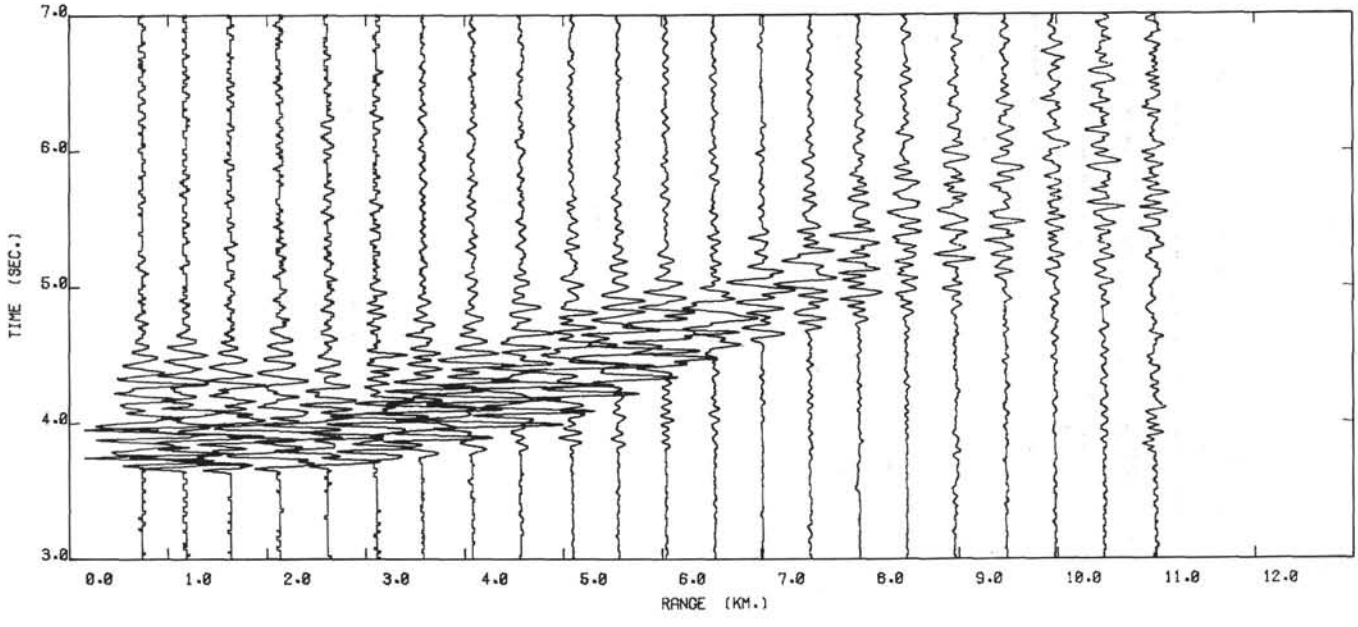

NORTH LINE - VERTICAL COMPONENT - D = 5840 M. BRF

LOW PASS FILTERED AT 30.00 HZ - REDUCTION VELOCITY OF 6.00 KM/SEC
AMPLITUDES WEIGHTED BY (R/7.0)**2.9 FOR R>7.0 KM.

Figure B-6a

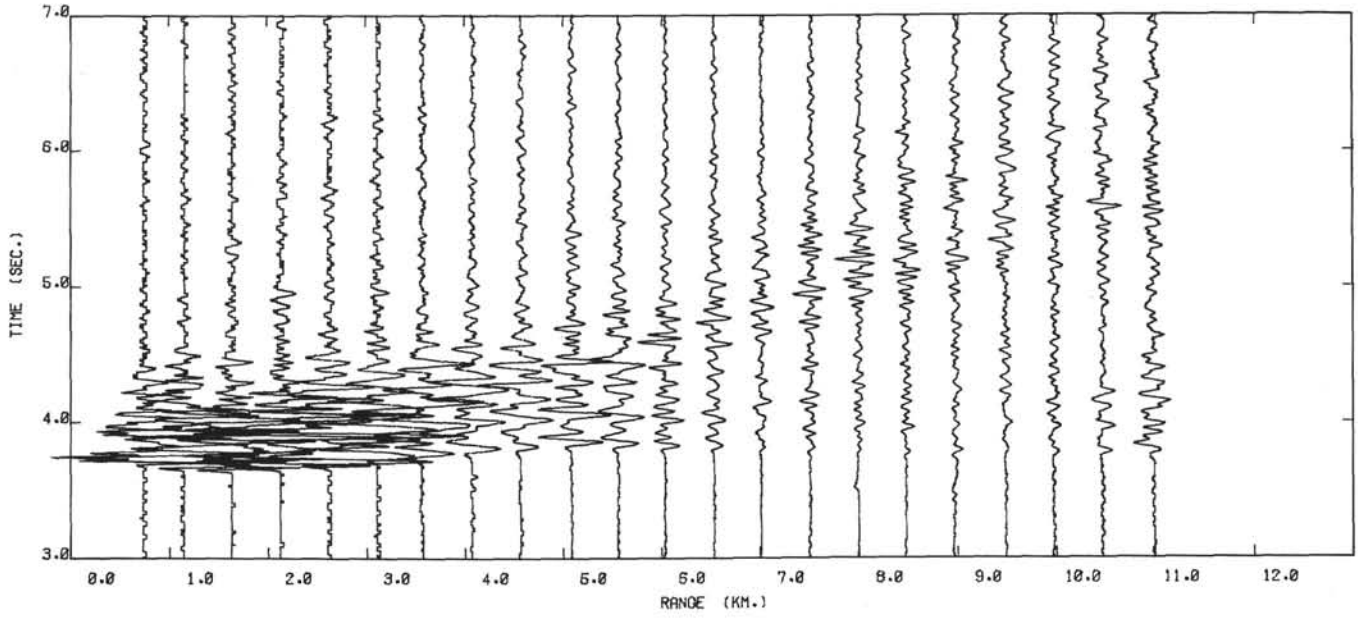

Figure B-6b

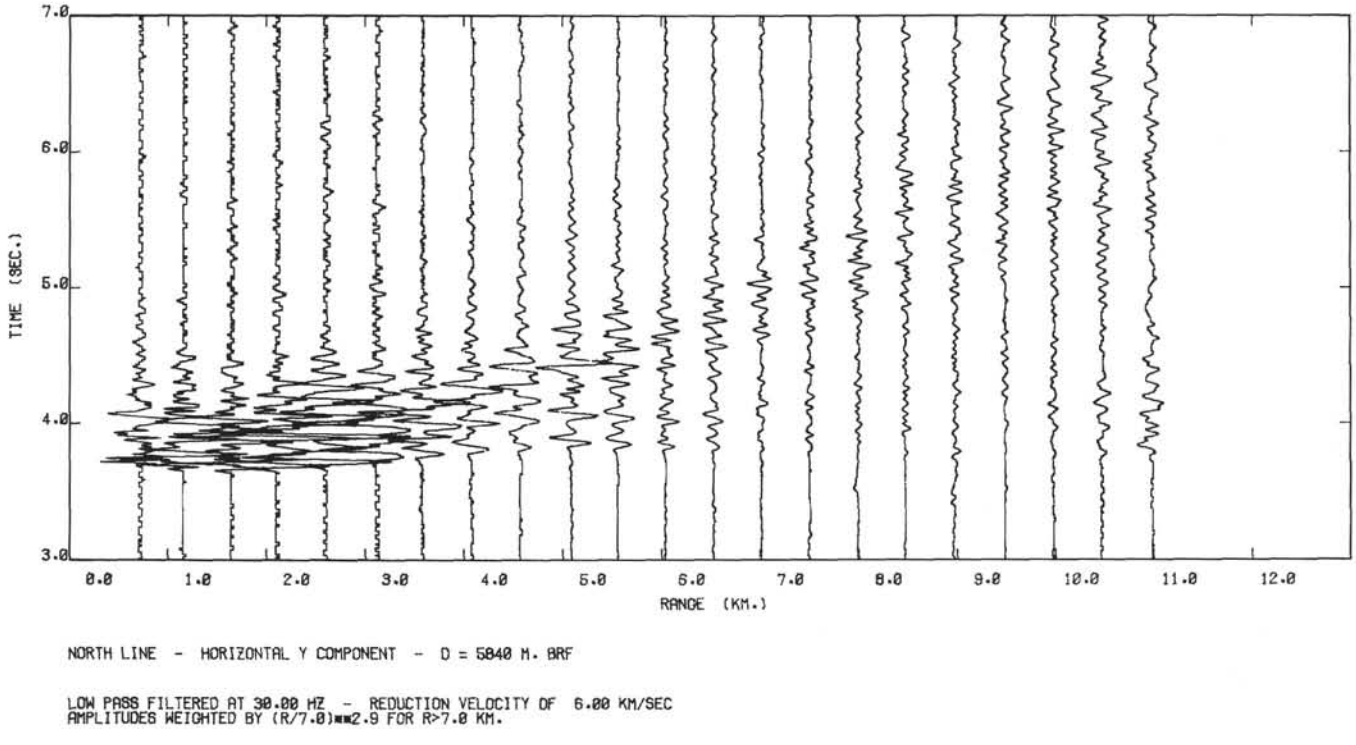

Figure B-6c

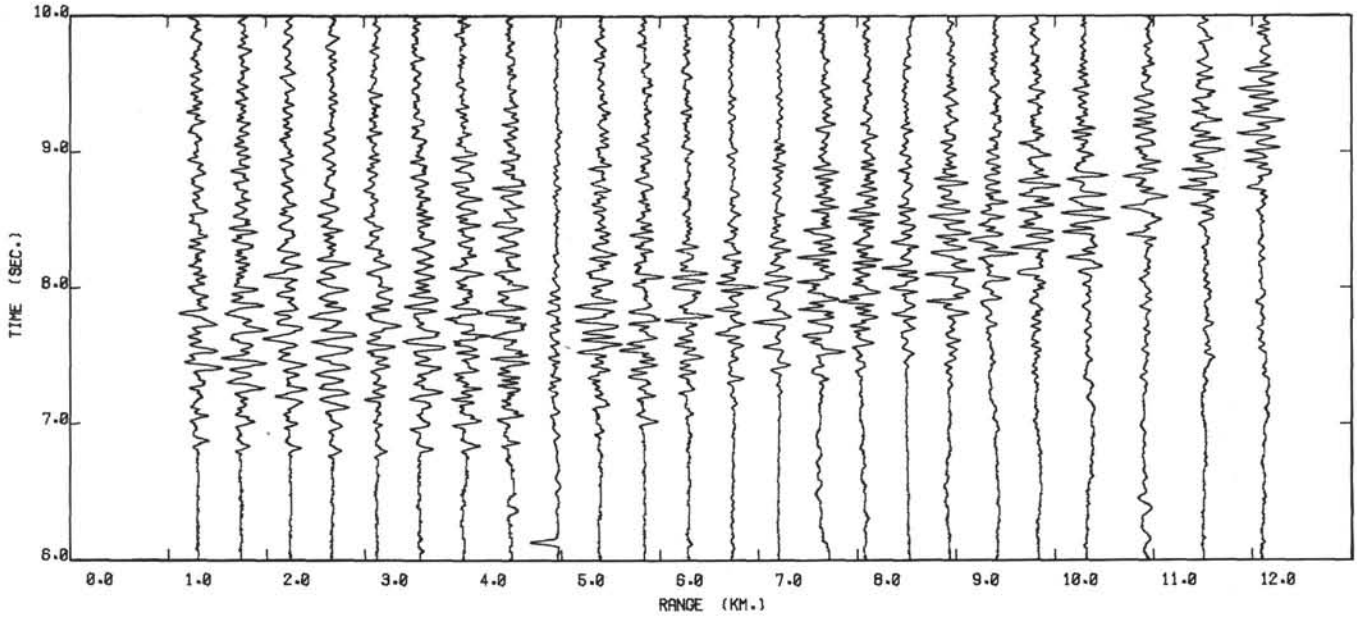

NORTH LINE - HYDROPHONE - D = 6060 M. BRF

LOW PASS FILTERED AT 30.00 HZ - REDUCTION VELOCITY OF 6.00 KM/SEC
INDIVIDUAL TRACES NORMALIZED TO A CONSTANT AMPLITUDE

Figure B-7a

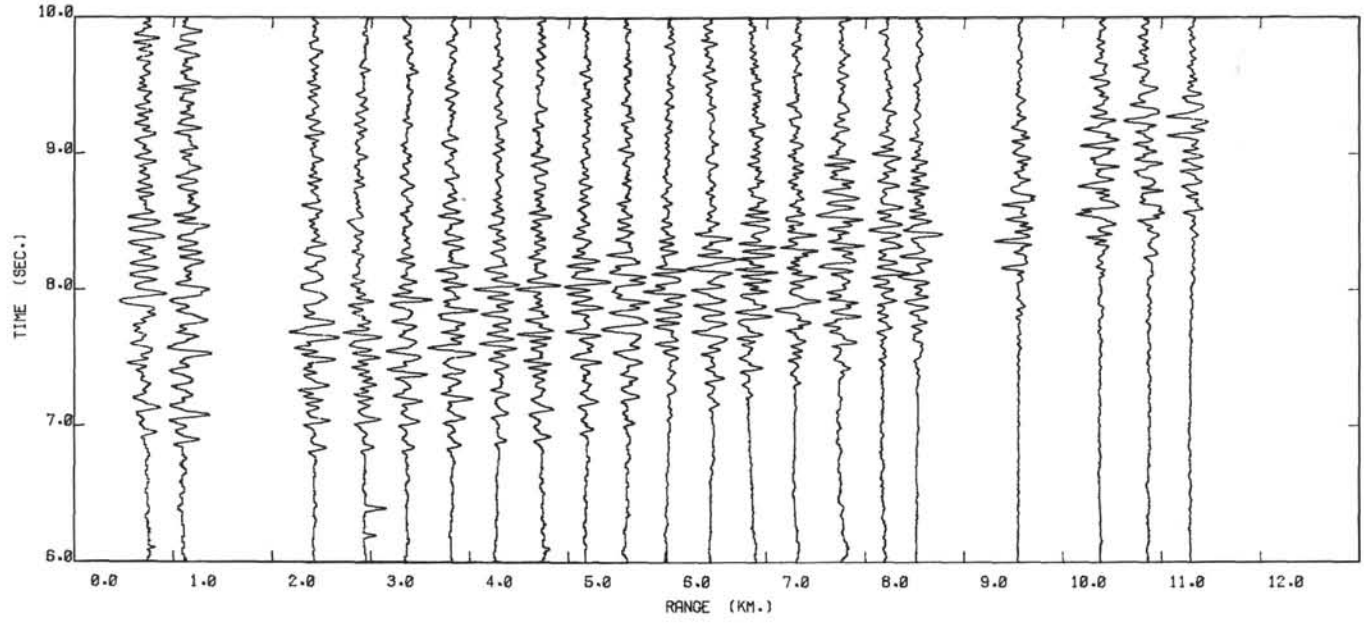

SOUTH LINE - HYDROPHONE - D = 6060 M. BRF

LOW PASS FILTERED AT 30.00 HZ - REDUCTION VELOCITY OF 6.00 KM/SEC
INDIVIDUAL TRACES NORMALIZED TO A CONSTANT AMPLITUDE

Figure B-7b

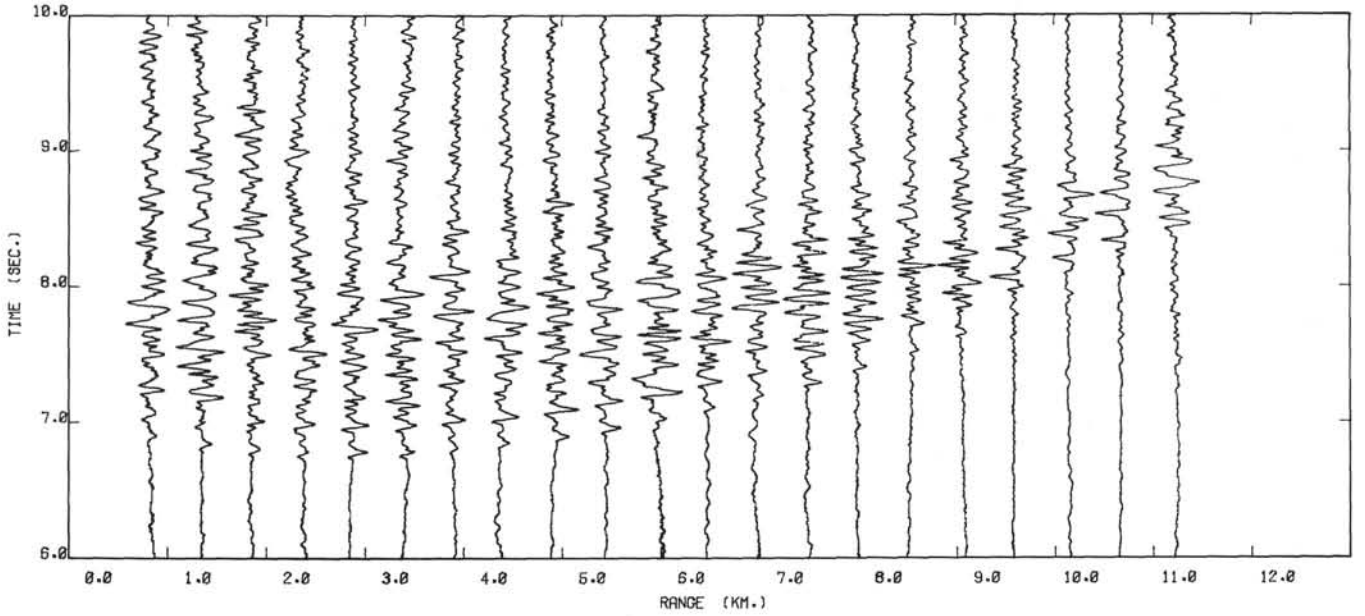

Figure B-7c

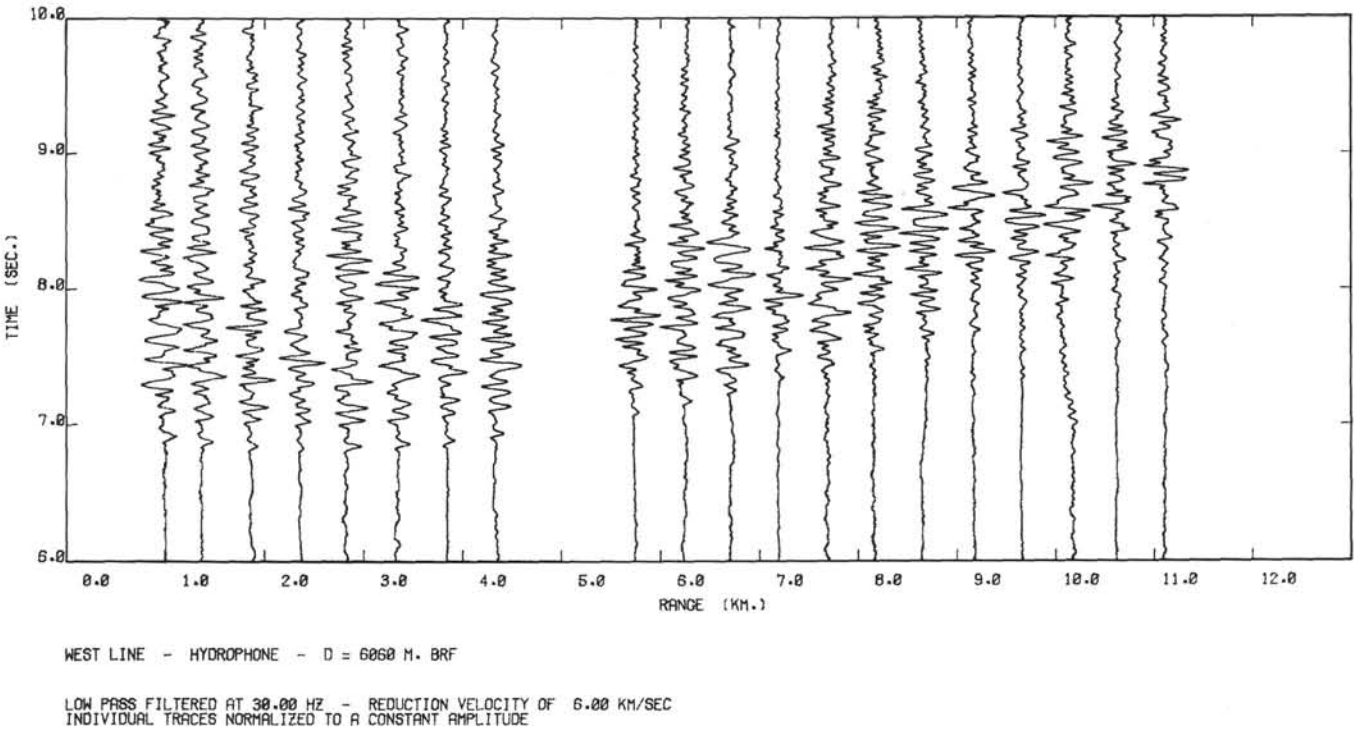

Figure B-7d

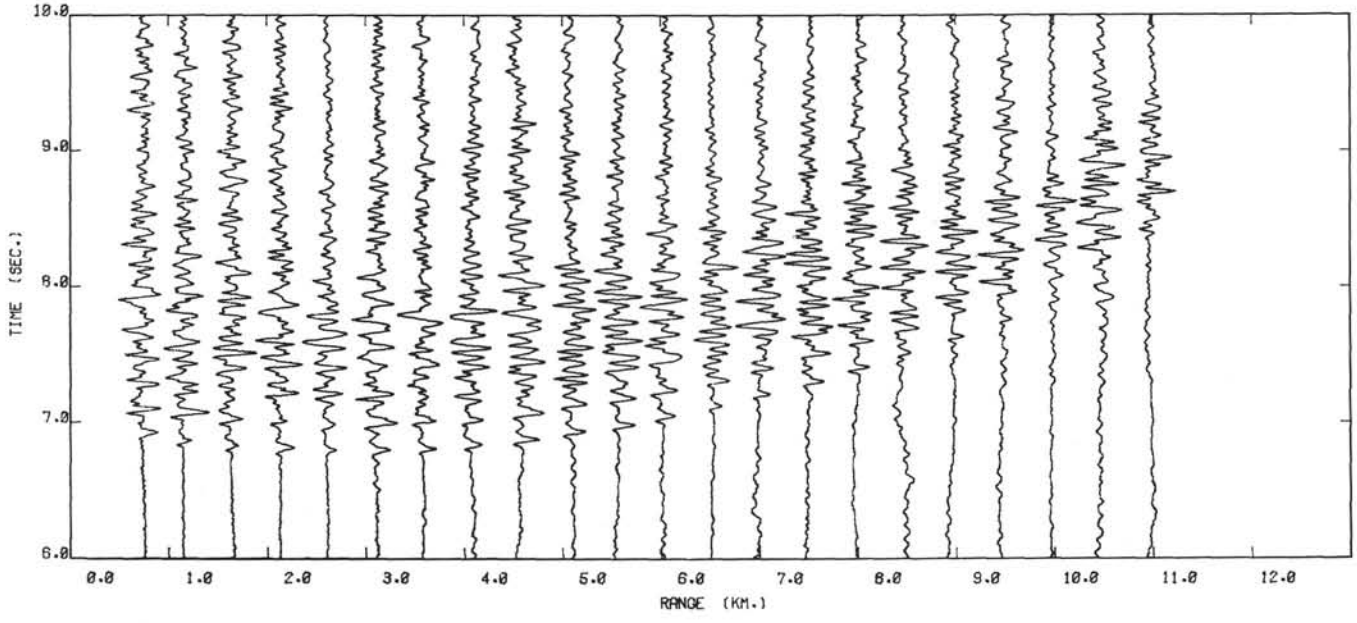

NORTH LINE - HYDROPHONE - D = 5840 M. BRF

LOW PASS FILTERED AT 30.00 HZ - REDUCTION VELOCITY OF 6.00 KM/SEC
INDIVIDUAL TRACES NORMALIZED TO A CONSTANT AMPLITUDE

Figure B-7e

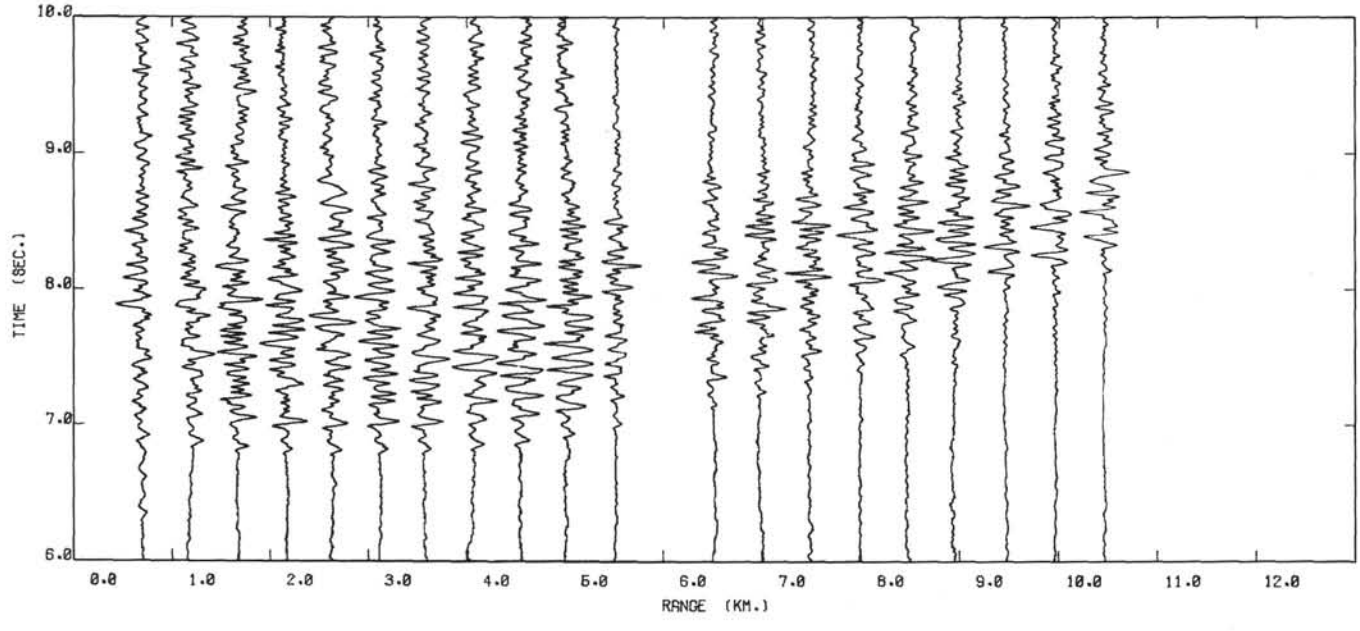

SOUTH LINE - HYDROPHONE - D = 5840 M. BRF

LOW PASS FILTERED AT 30.00 HZ - REDUCTION VELOCITY OF 6.00 KM/SEC
INDIVIDUAL TRACES NORMALIZED TO A CONSTANT AMPLITUDE

Figure B-7f

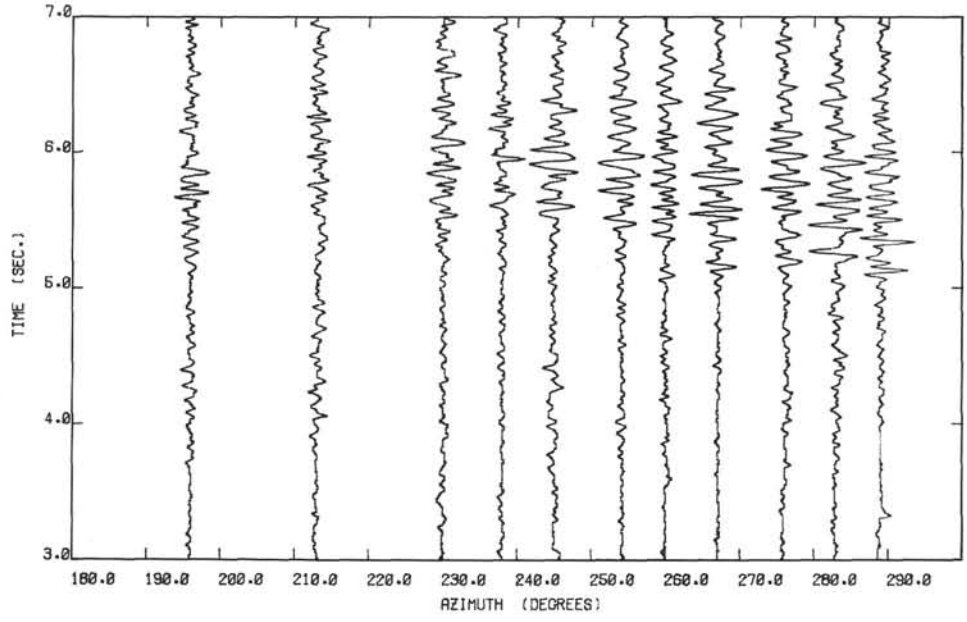

Figure B-8a

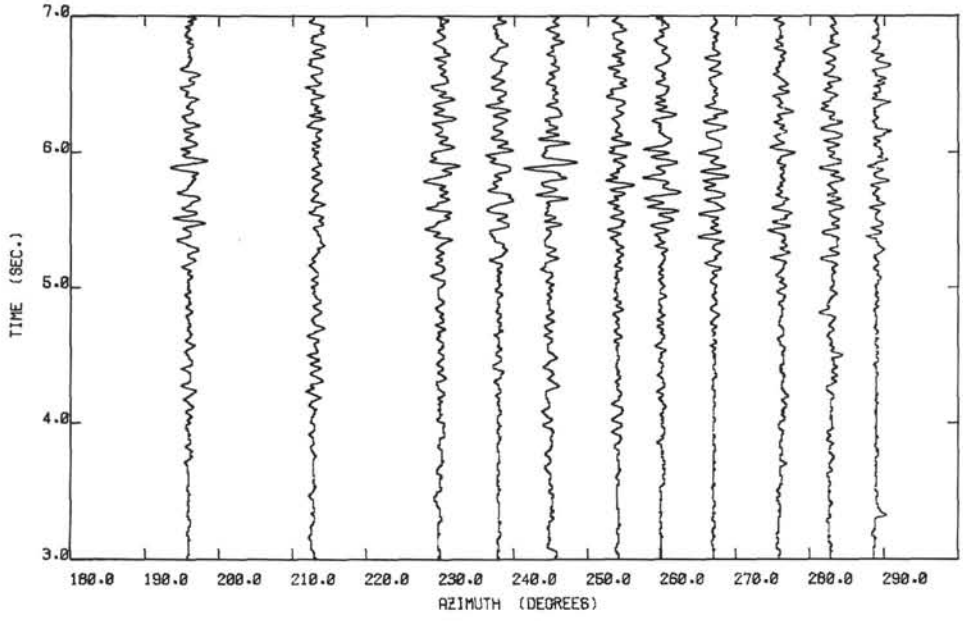

Figure B-8b

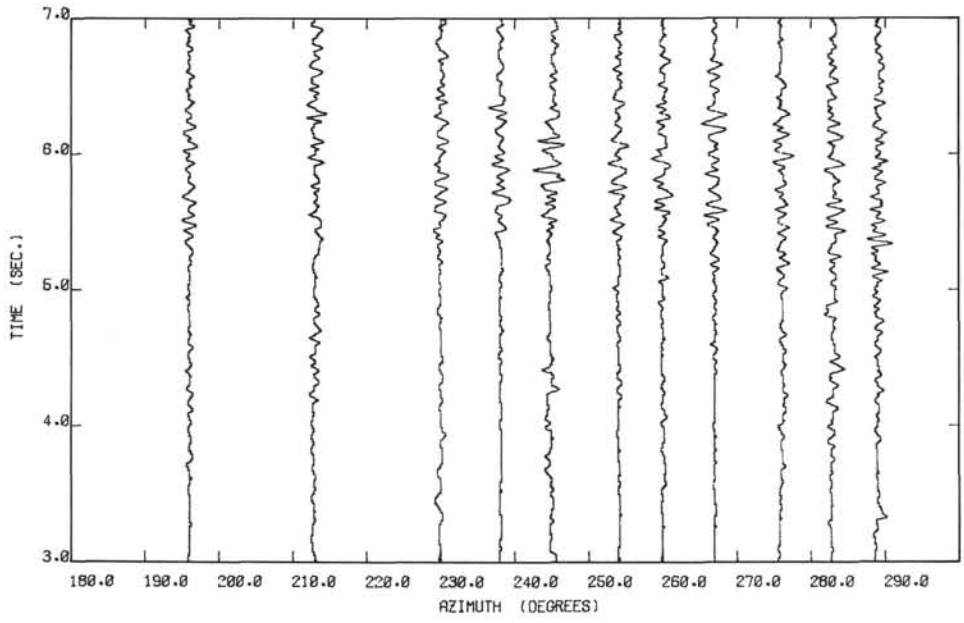

Figure B-8c

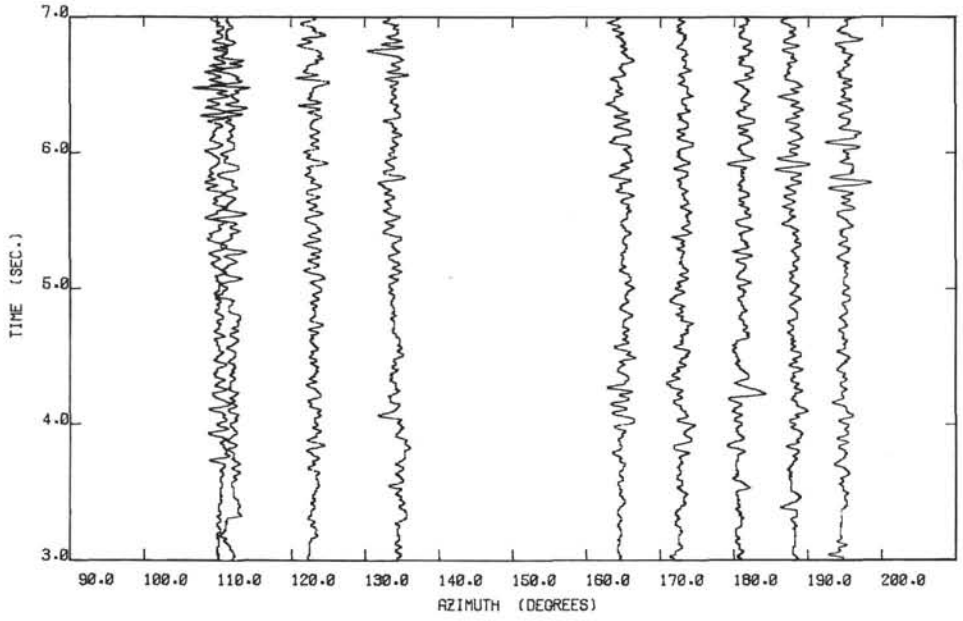

Figure B-9a

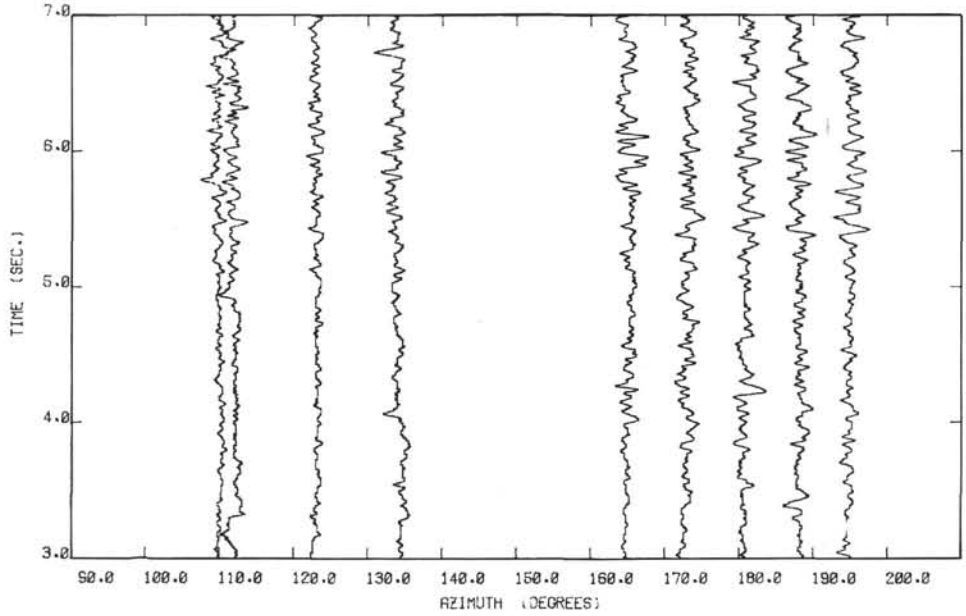

Figure B-9b

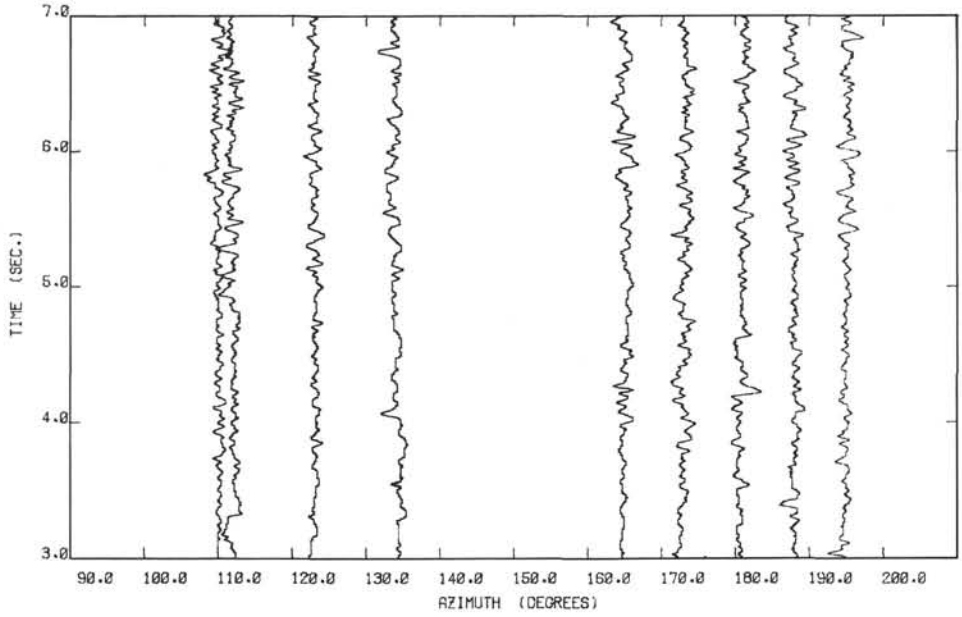

Figure B-9c